FACULDADE DE ENGENHARIA DA UNIVERSIDADE DO PORTO

Light localization in two-dimensional moiré lattices

José Pedro Afonso Gomes Luís

Mestrado em Engenharia Eletrotécnica e de Computadores

Supervisor: Maria Inês Barbosa de Carvalho

July 31, 2023

Resumo

Padrões de moiré têm numerosas aplicações em diferentes áreas. Em sistemas físicos, padrões de moiré têm sido aplicados em variados cenários, e muitas propriedades interessantes emergem nesses sistemas. Em particular, uma onda que se propaga num potencial suportado por uma rede de moiré pode estar localizada se essa rede for aperiódica (incomensurável). Se for periódica (comensurável), todos os modos lineares do sistema são ondas de Bloch, que são deslocalizadas por definição. Também foi mostrado que redes de moiré aperiódicas podem ser aproximadas por periódicas, e essas aproximações apresentam bandas extremamente achatadas. Além disso, foi observado que é possível localizar ondas nas fronteiras ou cantos de uma rede de moiré periódica.

Na literatura, redes de moiré quadradas e hexagonais têm sido aplicadas a variados sistemas físicos, mas redes de moiré baseadas em outras redes de Bravais raramente são mencionadas neste contexto. Assim, este trabalho pretende estudar redes de moiré quadradas, hexagonais, retangulares e retangulares centradas, e resumir as suas propriedades no contexto da propagação de ondas, utilizando a equação linear de Schrödinger. Para tal, uma metodologia foi cuidadosamente projetada, de modo a permitir resolver a equação para diferentes potenciais e condições de fronteira.

Mostra-se que redes de moiré retangulares e retangulares centradas podem ser periódicas numa dimensão quando certas condições se verificam. Neste caso, localização numa dimensão é possível. Além disso, para certas redes de moiré retangulares centradas, variar a intensidade das subredes é suficiente para causar uma transição de deslocalizado para localizado a uma dimensão, e de localizado a uma dimensão para localizado. Assim, redes de moiré retangulares e retangulares centradas apresentam propriedades únicas quando comparadas com redes de moiré quadradas ou hexagonais.

Também se mostra que, para redes de moiré quadradas, a localização na fronteira parece apenas ser possível em redes periódicas com fronteiras periódicas.

Abstract

Moiré patterns have numerous applications in various fields. In physical systems, moiré patterns have been applied in a variety of scenarios, and many interesting properties emerged in those systems. In particular, a wave propagating on a potential supported by a moiré lattice can be localized if that lattice is aperiodic (incommensurable). If it is periodic (commensurable), all linear modes of the system are Bloch waves, which are unlocalized by definition. It was also shown that aperiodic moiré lattices can be approximated by periodic ones, and those approximations present extremely flat bands. Additionally, it was observed that waves can be localized at the edges or corners of a periodic moiré lattice.

In the literature, square and hexagonal moiré lattices have been applied to various physical systems, but moiré lattices based on other Bravais lattices are rarely mentioned in this context. As such, this work aims to study square, hexagonal, rectangular, and centered rectangular moiré lattices, and summarize their properties in the context of wave propagation, using the linear Schrödinger equation. To do so, a methodology was carefully designed, such that the equation can be solved for different potentials and boundary conditions.

It is shown that rectangular and centered rectangular moiré lattices can be one-dimensional periodic when specific conditions are verified. In this case, localization in one dimension is possible. Additionally, for certain centered rectangular moiré lattices, varying the intensity of the sublattices is enough to transition from unlocalized to one-dimensional localized and from one-dimensional localized to localized. Thus, rectangular and centered rectangular moiré lattices present unique properties when compared to square and hexagonal ones.

It is also shown that, for square moiré lattices, edge localization only seems to be possible in periodic lattices with periodic edges.

Agradecimentos

Em primeiro lugar, agradeço à minha orientadora, Professora Maria Inês Carvalho, não só pela oportunidade de realizar este trabalho, mas também pela sua ajuda, disponibilidade e conhecimento partilhado.

À minha família, em especial aos meus pais, pela motivação, suporte e paciência que tiveram comigo, e ao meu irmão, pelo apoio e por me acompanhar sempre.

Aos meus amigos que me acompanharam ao longo do percurso académico.

A todos os professores da Faculdade de Engenharia da Universidade do Porto, pelo conhecimento partilhado.

À Faculdade de Engenharia da Universidade do Porto, por todas as oportunidades de aprendizagem que me proporcionou.

Ao INESC TEC, pela oportunidade de realizar esta dissertação.

À FCT, por financiar o projeto "Ondas de Matéria em Redes Moiré", com a referência PTDC/FIS-OUT/3882/2020, onde este trabalho se insere.

José Pedro Luís

"Para ser grande, sê inteiro: nada
Teu exagera ou exclui.
Sê todo em cada coisa. Põe quanto és
No mínimo que fazes."

Ricardo Reis

Contents

List of Figures

List of Tables

Chapter 1

Introduction

1.1 Context

Throughout the years, moiré patterns, that is, interference patterns created by the superimposition of two different periodic patterns, have been applied in the most diverse areas such as "artistic design, the textile industry, architecture, image processing, metrology and interferometry" [4, p. 42].

In physics, it was observed that moiré patterns substantially change the behavior of systems. For example, it has been studied in the context of the quantum Hall effect [5], unconventional superconductivity [6, 7, 8], and photorefractive crystals, including soliton formation [4, 9, 10].

When it comes to localization, it is known that a periodic potential only allows Bloch modes, which are unlocalized [11]. Also, disordered systems may have Anderson localization [12]. Aperiodic systems do not fit in any of these cases and many interesting behaviors have been observed. In particular, moiré lattices may be aperiodic, in which case they support localized states [3]. Additionally, these moiré lattices may be approximated by periodic ones, and these approximations present extremely flat bands when localization occurs [4].

1.2 Motivation

Wave localization is relevant for numerous applications. With moiré lattices, it is possible to control wave localization in a physical system by tuning the lattice parameters. Recent photonic applications include narrow band filter design [13], propagation of light bullets [14], silicon photonic nanowires [15], narrow optical resonances [16], high harmonic generation [17], a photonic crystal fiber [18], and light trapping in photonic crystal slabs [19].

Most studies are focused on square moiré lattices, due to their simplicity, or hexagonal ones, which can be observed in graphene. It is thus relevant to study and summarize the properties associated with wave localization in potentials supported by moiré lattices based on these and other Bravais lattices, more precisely: square, hexagonal, rectangular, and centered rectangular.

1.3 Objectives

The main objective of this work is to study light localization in potentials supported by moiré lattices which are either periodic or aperiodic. This study consists of:

- Determining the conditions that define whether a moiré lattice is periodic or aperiodic;
- Computing the propagation modes and band structure associated with potentials supported by periodic moiré lattices;
- Computing the propagation modes in potentials supported by periodic or aperiodic moiré lattices, in a finite region, and an objective measure of localization to compare the localization of different modes.

1.4 Document Structure

After this introductory chapter, this document consists of seven more chapters. Chapter 2 explores in more detail some fundamental aspects related to this work. Chapter 3 consists of a review of the state-of-the-art. Chapter 4 describes the most relevant aspects of the methodology that was designed to solve the problem. Chapter 5 presents theoretical aspects as well as examples related to periodic moiré lattices, in particular, square, hexagonal, rectangular and centered rectangular moiré lattices. These examples are then further developed in Chapters 6 and 7. The former focuses on light localization in the center of a finite region, with a potential supported by a moiré lattice (periodic or aperiodic), defined as the superimposition of cosines. The latter explores light localization at the edges or corners of a finite region, with a potential that is similar to the former, but its definition is based on the repetition of gaussian functions and it is truncated. Chapter 8 is the final chapter, where the main conclusions are presented, and future work is discussed.

Chapter 2

Background and Fundamental Aspects

2.1 Bravais Lattices and Reciprocal Lattices

A Bravais lattice is, in three-dimensional space, an infinite set of points which present translational symmetry along those dimensions. Thus, there are three fundamental spatial periods $\mathbf{a}_1$, $\mathbf{a}_2$, and $\mathbf{a}_3$, which can be combined with integer coefficients n_1, n_2, and n_3, respectively, to create any period vector $\mathbf{R}$:

$$\mathbf{R} = n_1\mathbf{a}_1 + n_2\mathbf{a}_2 + n_3\mathbf{a}_3 \tag{2.1}$$

Based on symmetry, these lattices can be divided into groups. There are five two-dimensional lattices divided into four groups, shown in Figure 2.1 and Table 2.1, respectively. In this work, four lattices are considered: square, hexagonal, rectangular, and centered rectangular.

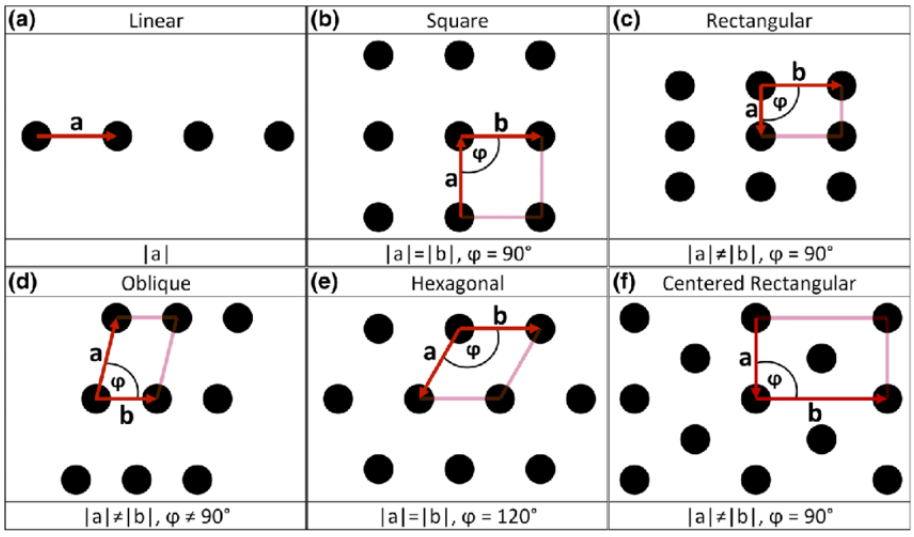

Figure 2.1: One- and two-dimensional Bravais lattices [1].

There are fourteen different three-dimensional Bravais lattices. For reference, the cubic lattices are presented in Figure 2.2.

Table 2.1: Groups of two-dimensional Bravais lattices

Group	Lattice types	
	Primitive	**Centered**
Monoclinic	Oblique	-
Orthorhombic	Rectangular	Centered rectangular
Tetragonal	Square	-
Hexagonal	Hexagonal	-

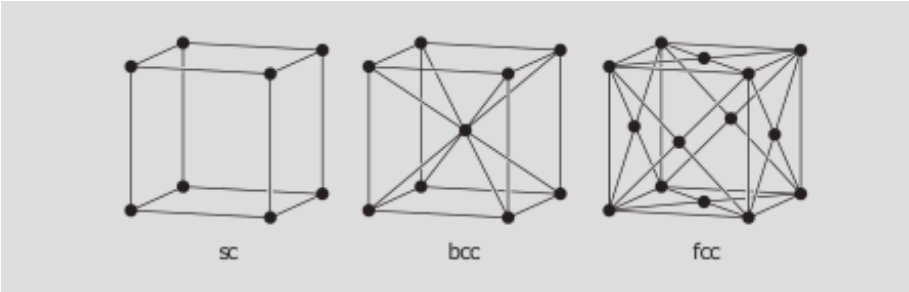

Figure 2.2: Cubic Bravais lattices [2].

A Bravais lattice is a discrete representation of the periodicity of a system's structure, for example, crystals. Some physical quantities in these systems will be periodic as well, and thus admit a Fourier series expansion. The domain of this expansion is a lattice itself, the reciprocal lattice, for which the typical primitive vectors are

$$\mathbf{b}_1 = 2\pi \frac{\mathbf{a}_2 \times \mathbf{a}_3}{V} \tag{2.2}$$

$$\mathbf{b}_2 = 2\pi \frac{\mathbf{a}_3 \times \mathbf{a}_1}{V} \tag{2.3}$$

$$\mathbf{b}_3 = 2\pi \frac{\mathbf{a}_1 \times \mathbf{a}_2}{V} \tag{2.4}$$

where $V = |\mathbf{a}_1 \cdot \mathbf{a}_2 \times \mathbf{a}_3|$ is the volume of the crystal.

The first Brillouin zone is the set of points in reciprocal space where every point is closer to the origin than any of its translations by a reciprocal lattice vector.

2.2 Moiré Patterns and Lattices

A moiré pattern is an interference pattern caused by the superimposition of periodic signals. Those signals may represent, for example, images or audio. The signals may also have a relative transformation before being combined, typically a translation or rotation. This pattern may then be periodic or aperiodic. In the context of this work, the signals are physical quantities, for example, electron concentration or refractive index. An example of a moiré pattern is presented in Figure 2.3.

A moiré lattice (sometimes called Bravais-moiré lattice in the literature [20, 13]) is a moiré pattern formed by the superimposition of two Bravais lattices. The resulting lattice may then be

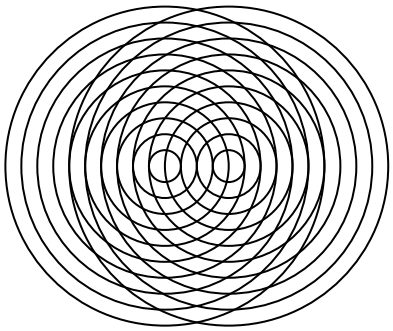

Figure 2.3: Example of a moiré pattern. The superimposition of two equal sets of concentric circles generates an interference pattern.

periodic or aperiodic. Figure 2.4 illustrates a square moiré lattice.

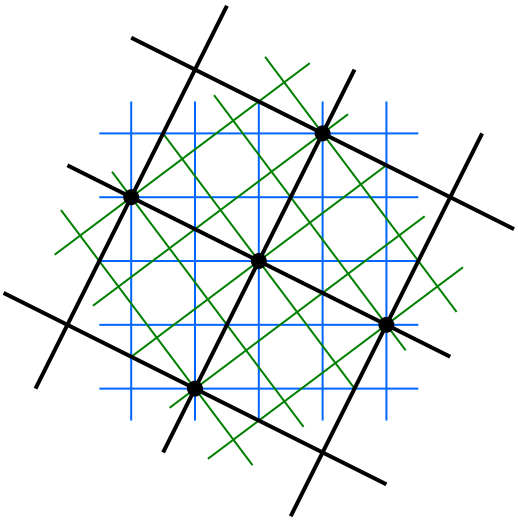

Figure 2.4: Example of a moiré lattice. The blue lines represent a square lattice, the green ones represent its rotated copy, and their superimposition generates a new lattice, which is also square, but with a larger area per square than the other two, represented by the black lines. The black dots mark the visible intersections of the two interfering lattices.

2.3 Band Theory

Band theory tries to explain the electronic behavior of crystals, in particular why there are metals, insulators, semimetals, and semiconductors. It defines the concept of bands, which correspond to allowed or forbidden energy levels within the crystal. The forbidden levels are usually called band gaps. These gaps are explained by the reflection of waves at reciprocal lattice boundaries.

The Bloch theorem is particularly relevant in band theory as it states that, for a periodic potential, all wave functions must be periodic in magnitude, with the same period as the potential, and are affected by a phase shift $\mathbf{k} \cdot \mathbf{r}$, where $\mathbf{k}$ is the wave vector and $\mathbf{r}$ is the position vector. These are called Bloch functions and can be written as

$$\psi_{\mathbf{k}}(\mathbf{r}+\mathbf{R}) = e^{j\mathbf{k}\cdot\mathbf{r}} u_{\mathbf{k}}(\mathbf{r}) \tag{2.5}$$

where $u_{\mathbf{k}}(\mathbf{r}+\mathbf{R}) = u_{\mathbf{k}}(\mathbf{r})$, so that

$$\psi_{\mathbf{k}}(\mathbf{r}+\mathbf{R}) = e^{j\mathbf{k}\cdot\mathbf{R}} \psi_{\mathbf{k}}(\mathbf{r}) \tag{2.6}$$

The bands result from the Schrödinger equation $\hat{H}\psi = E\psi$, where $\hat{H}$ is the Hamiltonian operator of the system and E is its energy. As an example, the equation for a one-electron approximation in a potential V becomes

$$\left(\frac{\hat{\mathbf{p}}^2}{2m} + V\right)\psi = E\psi \tag{2.7}$$

where $\hat{\mathbf{p}} = -j\hbar\nabla$ is the momentum operator of the electron, and m is its mass.

If a potential V is periodic, it can be written as a Fourier series expansion, with coefficients $V_{\mathbf{G}}$:

$$V = \sum_{\mathbf{G}} V_{\mathbf{G}} e^{j\mathbf{G}\cdot\mathbf{r}} \tag{2.8}$$

where the summation is over all reciprocal lattice vectors $\mathbf{G}$. Additionally, ψ is a Bloch function and therefore it can be written as a plane wave expansion, with coefficients $C_{\mathbf{k}}$:

$$\psi = \sum_{\mathbf{k}} C_{\mathbf{k}} e^{j\mathbf{k}\cdot\mathbf{r}} \tag{2.9}$$

where the summation is over all wave vectors $\mathbf{k}+\mathbf{G}$. Substituting ψ and V with the corresponding expansions in Equation 2.7 and simplifying yields the central equation [2]:

$$\left(\frac{\hat{\mathbf{p}}^2}{2m} - E\right) C_{\mathbf{k}} + \sum_{\mathbf{G}} V_{\mathbf{G}} C_{\mathbf{k}-\mathbf{G}} = 0 \tag{2.10}$$

In the empty lattice approximation, all wave vectors $\mathbf{k}$ are moved to the first Brillouin zone with a suitable lattice vector $\mathbf{G}$. It is then possible to compute the eigenvalues E for each $\mathbf{k}$, which results in a band structure, for example, the one presented in Figure 2.5.

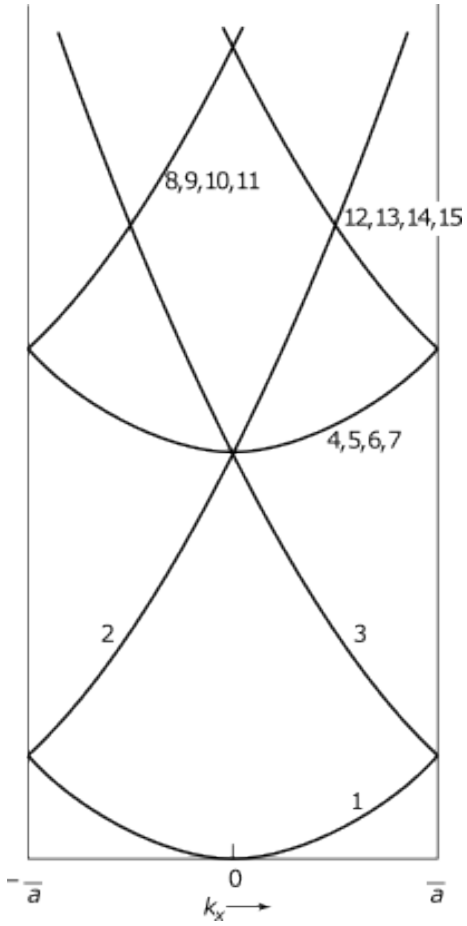

Figure 2.5: Example of free electron energy bands of the empty simple cubic lattice [2].

Chapter 3

Literature Review

3.1 Moiré Lattices

In the literature, moiré lattices are typically square or hexagonal, i.e. created by superimposing a square or hexagonal Bravais lattice, respectively, with its rotated copy. On the one hand, graphene is a hexagonal lattice and, as such, it is possible to obtain a hexagonal moiré lattice by superimposing two graphene layers, which leads to very interesting properties [6, 7, 8, 21, 22]. On the other hand, square lattices are very simple, so that, in scenarios where the lattice geometry can be chosen, in particular, photonic moiré lattices, it is often used [4, 9, 10, 13, 20, 23].

3.1.1 Square

A square moiré lattice is the superimposition of a square lattice with its rotated copy. Figure 3.1 illustrates three examples of potentials supported by square moiré lattices.

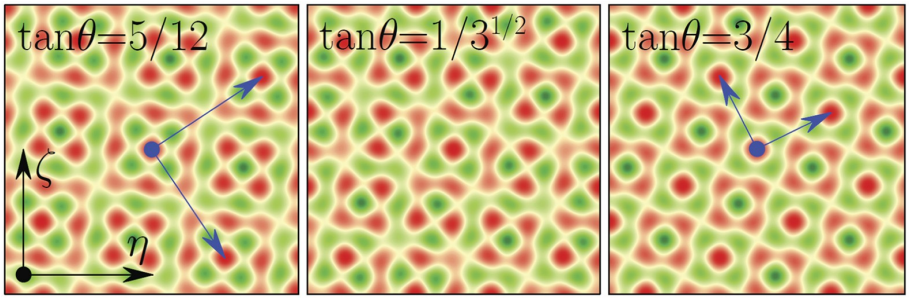

Figure 3.1: Resulting potential for the superimposition of two square lattices, which can be periodic (first and third columns) or aperiodic (second column) [3].

Let θ be the rotation angle. Then, according to [3], the resulting lattice is periodic if

$$\tan(\theta) = \frac{b}{a} \tag{3.1}$$

where $a, b \in \mathbb{Z}$ correspond to a solution of the equation

$$a^2 + b^2 = c^2 \tag{3.2}$$

where $c \in \mathbb{Z}$. The last equation is a Diophantine equation because the solutions must be integer numbers.

3.1.2 Hexagonal

A hexagonal moiré lattice is similar to a square moiré lattice, but the lattice and its rotated copy are hexagonal lattices. Figure 3.2 shows three examples of potentials supported by hexagonal moiré lattices.

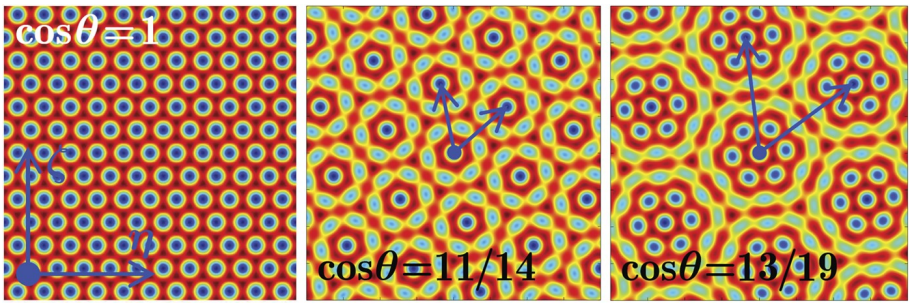

Figure 3.2: Resulting potential for the superimposition of two hexagonal lattices, which is equal to the original lattices for $\theta = 0$ (first column) and periodic for angles that verify the condition (second and third columns) [3].

It is also possible to obtain conditions for θ [3], such that the resulting lattice is periodic if

$$\tan(\theta) = \sqrt{3}\frac{b}{2a+b} \tag{3.3}$$

where $a, b \in \mathbb{Z}$ correspond to a solution of the equation

$$a^2 + ab + b^2 = c^2 \tag{3.4}$$

where $c \in \mathbb{Z}$. Again, the last equation is a Diophantine equation.

3.2 Moiré Potential

In this context, the potential is a continuous function $V(x,y)$ along the space coordinates $\mathbf{r} = (x,y)$. A moiré potential is obtained by superimposing two potentials supported by Bravais lattices, such that the resulting potential is supported by a moiré lattice.

In [3], it is defined as

$$V(\mathbf{r}) = V_1(\mathbf{r}) + \frac{p_2}{p_1}V_1(\mathbf{r}) \tag{3.5}$$

where p_1 and p_2 are the intensities of the first and second sublattice, respectively, S is the rotation matrix for angle θ,

$$S = \begin{bmatrix} \cos(\theta) & -\sin(\theta) \\ \sin(\theta) & \cos(\theta) \end{bmatrix} \tag{3.6}$$

and $V_1(\mathbf{r})$ is the first sublattice potential, defined as

$$V_1(\mathbf{r}) = p_1[\cos(2x) + \cos(2y)] \tag{3.7}$$

In [4], it is the potential associated with the experimental setup, given by

$$V(\mathbf{r}) = -\frac{E_0}{1 + I(\mathbf{r})} \tag{3.8}$$

where E_0 is the dimensionless DC field, and $I(\mathbf{r})$ is the intensity

$$I(\mathbf{r}) = \left| p_1 V'(\mathbf{r}) + p_2 V'(S\mathbf{r}) \right|^2 \tag{3.9}$$

where p_1, p_2, S are similar to the previous case, and $V' = V_1/p_1$.

3.3 Wave Equation

The wave equation is the dimensionless Schrödinger equation [3, 4]:

$$j\frac{\partial \psi(\mathbf{r},z)}{\partial z} = -\frac{1}{2}\nabla_\perp^2 \psi(\mathbf{r},z) - V(\mathbf{r})\psi(\mathbf{r},z) \tag{3.10}$$

where ψ is the wave function, z is the propagation direction, $V(\mathbf{r})$ is the potential defined in the lattice plane, and $\nabla_\perp^2 = \frac{\partial^2}{\partial x^2} + \frac{\partial^2}{\partial y^2}$ is the Laplacian in that plane.

The considered linear modes are of the form

$$\psi(\mathbf{r},z) = w(\mathbf{r})\, e^{j\beta z} \tag{3.11}$$

where β is the propagation constant. Then, the wave equation is

$$-\beta w = -\frac{1}{2}\nabla_\perp^2 w - Vw \tag{3.12}$$

This is an eigenvalue problem, where β is the eigenvalue and w is the eigenfunction.

3.4 Band Structure

If the potential V is periodic, all solutions of Equation 3.12 are Bloch waves. Using the concepts of band theory (Section 2.3), it is possible to obtain the propagation constants β associated with each wave vector $\mathbf{k}$, resulting in a band structure. An example is presented in Figure 3.3.

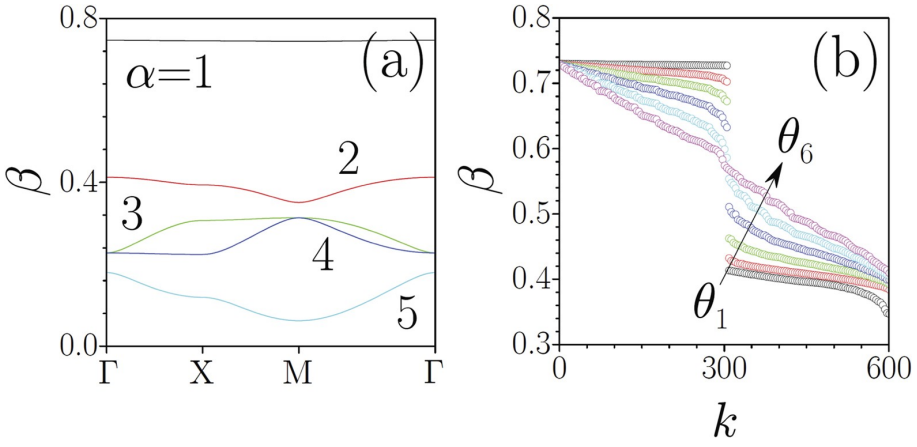

Figure 3.3: **(a)** Computed bands for a periodic potential with $\tan(\theta) = 3/4$, $p_1 = 1$ and $p_2 = 0.4$, in descending order of propagation constant β. **(b)** Evolution of the 600 largest propagation constants β_k associated with the top two bands ($\alpha = 1$ and $\alpha = 2$), for small variations of the rotation angle given by $\theta_n = \arctan(3/4) + n\pi/1800$ [3].

Additionally, aperiodic moiré potentials are quasiperiodic and, as such, they may be approximated by periodic moiré potentials, with an approximation error that decreases as the considered primitive cell area increases [4].

3.5 Measure of Localization

To measure the localization of a wave profile, both [3, 4] use the integral form factor χ, given that it is inversely proportional to the mode width. It can be computed as

$$\chi = \frac{\left(\iint |\psi|^4 d^2\mathbf{r}\right)^{\frac{1}{2}}}{\iint |\psi|^2 d^2\mathbf{r}} \tag{3.13}$$

This measure is useful to compare the localization of different wave profiles, as well as obtaining relevant characteristic curves such as the ones presented in Figures 3.4 and 3.5

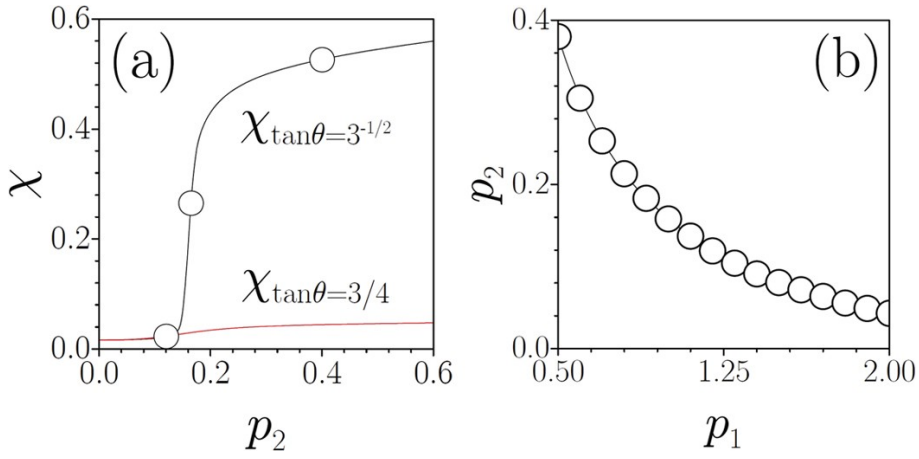

Figure 3.4: **(a)** Form factor for rotation angles corresponding to a periodic potential and a quasi-periodic potential, which shows that it is possible to localize light in a quasi-periodic potential, unlike periodic potentials. **(b)** Curve of p_1 vs. p_2 for a given rotation angle ($\theta = \pi/6$) and form factor value ($\chi = 0.1$). [3]

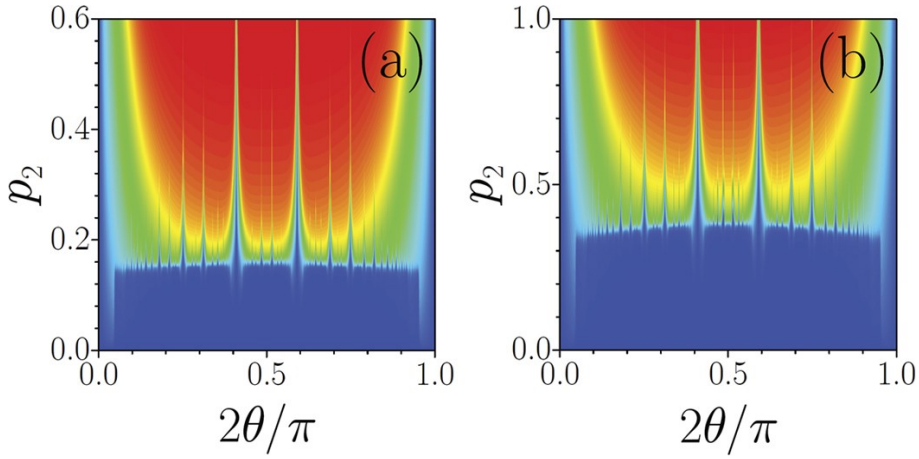

Figure 3.5: Form factor vs. p_2 vs. θ for **(a)** $p_1 = 1$ and **(b)** $p_1 = 0.5$. It is relevant to note that there is an approximately constant line for p_2 above which localization occurs, and also that some particular angles (corresponding to periodic potentials) are unable to localize light for arbitrarily large p_2. [3]

3.6 Localization in Moiré Lattices

Although other propagation modes are referred in [3, 4], wave localization is mostly discussed for the mode with the largest β, as it is the mode associated with the flattest band. This mode is localized in aperiodic moiré lattices and delocalized otherwise. However, [23] shows that other propagation modes can be localized in the edges and corners of a truncated periodic moiré lattice. This moiré lattice is truncated with a periodic edge, so two cases are not covered: periodic lattice with aperiodic edge, and aperiodic lattice, which implies aperiodic edges.

3.7 Summary

The literature extensively covers square and hexagonal moiré lattices. However, rectangular and centered rectangular moiré lattices are rarely mentioned, so it is relevant to explore them as well.

In the context of wave propagation, a lattice describes the periodicity of a potential. When a moiré lattice is periodic, only Bloch waves exist, and these are unlocalized by definition, although their magnitude may be confined to a small region of the primitive cell. As such, aperiodic moiré lattices, which can be approximated by periodic ones, also have similar modes, although they are aperiodic and, therefore, localized.

Finally, wave localization can also occur in the edges or corners of a periodic moiré lattice. These modes are localized due to lattice truncation in those edges. The described truncation was performed on periodic moiré lattices with periodic edges, but the other two cases should be studied: periodic lattices with aperiodic edges, and aperiodic lattices with aperiodic edges.

Chapter 4

Methodology

The main objective of this work is to compute relevant solutions of Equation 3.12, which is rewritten as follows:

$$\beta q = \frac{1}{2}\nabla_{\perp}^{2} q + V q \tag{4.1}$$

This chapter describes the approach used to solve this equation in Cartesian coordinates, for different boundary conditions. The algorithm, at a high level, comprises the following steps:

1. Create a normalized coordinates space, called UV space (Section 4.1);
2. Transform UV coordinates to lattice coordinates (UV1 and UV2);
3. Compute the discretization of V using UV, UV1 and UV2;
4. According to the chosen numerical method:
    - Finite differences
        (a) Create the matrix corresponding to the eigenvalues problem;
        (b) Compute the eigenvalues and eigenvectors of the matrix.
    - Plane wave decomposition
        (a) Compute the 2D FFT of V;
        (b) Create the matrix corresponding to the eigenvalues problem;
        (c) Compute the eigenvalues and eigenvectors of the matrix;
        (d) Convert the results to UV space.

This algorithm may be executed multiple times according to a higher-level algorithm that defines the steps to perform a certain lattice analysis (described in Section 4.4).

4.1 Normalized Coordinates

To simplify the computation of the PDE solutions, a normalized vector space is created, with variables u and v such that

$$\mathbf{r} = u\mathbf{a}_1 + v\mathbf{a}_2 \tag{4.2}$$

This is a very convenient definition, both for periodic and aperiodic potentials, as long as the region of interest is a parallelogram. For periodic potentials, $\mathbf{a}_1$ and $\mathbf{a}_2$ are the primitive lattice vectors and the period of coordinates u and v is 1.

To simplify some results in the following sections, it is also convenient to define the basis matrix:

$$A = \begin{bmatrix} \mathbf{a}_1 & \mathbf{a}_2 \end{bmatrix} \tag{4.3}$$

$$\begin{bmatrix} x \\ y \end{bmatrix} = A \begin{bmatrix} u \\ v \end{bmatrix} \tag{4.4}$$

Similar concepts can be defined for each superimposed Bravais lattice:

$$A_1 = \begin{bmatrix} \mathbf{a}_1^{(1)} & \mathbf{a}_2^{(1)} \end{bmatrix} \qquad A_2 = \begin{bmatrix} \mathbf{a}_1^{(2)} & \mathbf{a}_2^{(2)} \end{bmatrix} \tag{4.5}$$

$$\begin{bmatrix} x \\ y \end{bmatrix} = A_1 \begin{bmatrix} u^{(1)} \\ v^{(1)} \end{bmatrix} \qquad \begin{bmatrix} x \\ y \end{bmatrix} = A_2 \begin{bmatrix} u^{(2)} \\ v^{(2)} \end{bmatrix} \tag{4.6}$$

where $\mathbf{a}_1^{(1)}$ and $\mathbf{a}_2^{(1)}$ are the primitive lattice vectors of the first lattice, and $\mathbf{a}_1^{(2)}$ and $\mathbf{a}_2^{(2)}$ are the primitive lattice vectors of the second. An important property of this definition is that the period of all coordinates $u^{(1)}$, $v^{(1)}$, $u^{(2)}$, or $v^{(2)}$ is 1.

It is also possible to rewrite the global normalized coordinates as normalized coordinates for each of the lattices:

$$\begin{bmatrix} u^{(1)} \\ v^{(1)} \end{bmatrix} = A_1^{-1} A \begin{bmatrix} u \\ v \end{bmatrix} \tag{4.7}$$

$$\begin{bmatrix} u^{(2)} \\ v^{(2)} \end{bmatrix} = A_2^{-1} A \begin{bmatrix} u \\ v \end{bmatrix} \tag{4.8}$$

4.1.1 Normalized Reciprocal Lattice Coordinates

When solving the PDE with Bloch's theorem, it is also convenient to define normalized coordinates in reciprocal space.

Let $\mathbf{b}_1$ and $\mathbf{b}_2$ be the primitive vectors of the reciprocal lattice, which can be written as a matrix

$$B = \begin{bmatrix} \mathbf{b}_1 & \mathbf{b}_2 \end{bmatrix} \tag{4.9}$$

These vectors verify the following condition:

$$\begin{aligned} B^T A &= 2\pi I \\ B &= 2\pi A^{-T} \end{aligned} \tag{4.10}$$

where I is the 2×2 identity matrix. Then, $\mathbf{k}$ can be expressed in normalized reciprocal coordinates:

$$\mathbf{k} = k_u \mathbf{b}_1 + k_v \mathbf{b}_2 \tag{4.11}$$

Let $\mathbf{r} = u\mathbf{a}_1 + v\mathbf{a}_2$. It follows that the dot product $\mathbf{k} \cdot \mathbf{r}$ is simply

$$\mathbf{k} \cdot \mathbf{r} = (k_u \mathbf{b}_1 + k_v \mathbf{b}_2) \cdot (u\mathbf{a}_1 + v\mathbf{a}_2) = 2\pi (k_u u + k_v v) \tag{4.12}$$

Additionally, $\mathbf{G}$ can be expressed in normalized reciprocal coordinates as well: $\mathbf{G} = g_u \mathbf{b}_1 + g_v \mathbf{b}_2$, and the results are similar to $\mathbf{k}$, although $g_u, g_v \in \mathbb{Z}$.

4.2 Finite Differences Method

The finite differences method consists of considering a discretization of the domain of the differential equation to be solved. In this case, it is a region in the xy plane, and the most convenient discretization depends on the boundary conditions.

4.2.1 Types of Boundary Conditions and Discretization

In this work, two types of boundary conditions are considered: Bloch and zero. Bloch boundary conditions are a direct application of Bloch's theorem (Equation 2.6), so the most appropriate discretization is along a primitive cell of the lattice. Zero boundary conditions consist of setting the value of the wave to 0 at the boundaries of the considered region.

In both cases, vectors $\mathbf{a}_1$ and $\mathbf{a}_2$ define the space of the discretization. For Bloch conditions, however, there are two additional requirements: these vectors must correspond to primitive lattice vectors, and the points for $u = 1$ and $v = 1$ are not considered, given that they belong to a different lattice cell.

Let N_u and N_v be the number of points to consider on the discretization of u and v, respectively. Then, the discretizations of $q(x,y)$ and $V(x,y)$ are

$$q_{n_u,n_v} = q(u_0 + n_u\Delta u, v_0 + n_v\Delta v) \tag{4.13}$$

$$V_{n_u,n_v} = V(u_0 + n_u\Delta u, v_0 + n_v\Delta v) \tag{4.14}$$

where, for u and v, respectively, u_0 and v_0 are the values where the considered region starts, Δu and Δv are the discretization steps, and $0 \leq n_u \leq N_u - 1$ and $0 \leq n_v \leq N_v - 1$ are the discrete variables.

For Bloch boundary conditions, the considered discretization is given by

$$u_0 = v_0 = -0.5 \qquad \Delta u = \frac{1}{N_u} \qquad \Delta v = \frac{1}{N_v}$$

For zero boundary conditions, it is given by

$$u_0 = -0.5 + \Delta u \qquad v_0 = -0.5 + \Delta v \qquad \Delta u = \frac{1}{N_u + 1} \qquad \Delta v = \frac{1}{N_v + 1}$$

4.2.2 Laplacian and Normalized Coordinates

Due to the use of normalized coordinates, the Laplacian operator has to be rewritten:

$$\nabla_\perp^2 = \nabla_{xy}^T \nabla_{xy} = \left(A^{-T}\nabla_{uv}\right)^T \left(A^{-T}\nabla_{uv}\right) = \nabla_{uv}^T A^{-1} A^{-T} \nabla_{uv} \tag{4.15}$$

This implies that the cross derivatives must be taken into account as well. It is convenient to define a matrix $M = A^{-1}A^{-T}$:

$$M = \begin{bmatrix} m_{11} & m_{12} \\ m_{21} & m_{22} \end{bmatrix} \tag{4.16}$$

The equation to be solved is then

$$\begin{aligned} \beta q(u,v) = & \frac{1}{2}\left(m_{11}\frac{\partial^2 q}{\partial u^2}(u,v) + (m_{12} + m_{21})\frac{\partial^2 q}{\partial v \partial u}(u,v) + m_{22}\frac{\partial^2 q}{\partial v^2}(u,v) \right) \\ & + V(u,v)\, q(u,v) \end{aligned} \tag{4.17}$$

4.2.3 Equation Written as Finite Differences

Using the appropriate discretization, and considering central finite differences of second-order accuracy, the second-order partial derivatives, can be written as

$$\frac{\partial^2 q}{\partial u^2}(u,v) \approx \frac{q_{n_u+1,n_v} - 2q_{n_u,n_v} + q_{n_u-1,n_v}}{(\Delta u)^2} \tag{4.18}$$

$$\frac{\partial^2 q}{\partial v^2}(u,v) \approx \frac{q_{n_u,n_v+1} - 2q_{n_u,n_v} + q_{n_u,n_v-1}}{(\Delta v)^2} \tag{4.19}$$

$$\frac{\partial^2 q}{\partial v \partial u}(u,v) \approx \frac{q_{n_u+1,n_v+1} - q_{n_u+1,n_v-1} - q_{n_u-1,n_v+1} + q_{n_u-1,n_v-1}}{4(\Delta u)(\Delta v)} \tag{4.20}$$

The equation, written using finite differences, is then

$$\begin{aligned}\beta q_{n_u,n_v} = &\frac{1}{2}\left(m_{11}\frac{q_{n_u+1,n_v}-2q_{n_u,n_v}+q_{n_u-1,n_v}}{(\Delta u)^2}+m_{22}\frac{q_{n_u,n_v+1}-2q_{n_u,n_v}+q_{n_u,n_v-1}}{(\Delta v)^2}\right.\\ &\left.+(m_{12}+m_{21})\frac{q_{n_u+1,n_v+1}-q_{n_u+1,n_v-1}-q_{n_u-1,n_v+1}+q_{n_u-1,n_v-1}}{4(\Delta u)(\Delta v)}\right)\\ &+V_{n_u,n_v}q_{n_u,n_v}\end{aligned} \tag{4.21}$$

There is an equation for each n_u, n_v in the considered region, so the problem can be written in matrix form as $\beta q = Hq$, which is an eigenvalue problem. The equations are not complete, though, as they depend on q_{n_u,n_v} for n_u, n_v outside the considered region, in particular, the points at the boundary. These values are defined by the boundary conditions.

4.2.4 Application of Boundary Conditions

4.2.4.1 Bloch

Using Equation 4.12, Bloch's theorem (Equation 2.6) can be expressed as

$$q(u+n_1, v+n_2) = e^{j2\pi(k_u n_1 + k_v n_2)} q(u,v) \tag{4.22}$$

For the considered discretization, it can be written as

$$q_{n'_u,n'_v} = e^{j2\pi(k_u n_1 + k_v n_2)} q_{n_u,n_v} \tag{4.23}$$

where $n'_u = n_1 N_u + n_u$ and $n'_v = n_2 N_v + n_v$, corresponding to integer division, and $n'_u, n'_v \in \mathbb{Z}$, such that $q_{n'_u,n'_v}$ is not restricted to the primitive cell.

4.2.4.2 Zero

The application of zero boundary conditions is straightforward: the coefficients corresponding to terms where q_{n_u,n_v} is not defined are set to 0.

4.3 Plane Wave Decomposition Method

The plane wave decomposition method can only be applied to periodic potentials, as it consists of converting the PDE to Fourier space. It consists of writing q as a plane wave expansion, and V as a Fourier series expansion, with coefficients $Q_{\mathbf{k}}$ and $V_{\mathbf{G}}$, respectively:

$$q(\mathbf{r}) = \sum_{\mathbf{k}} Q_{\mathbf{k}} e^{j\mathbf{k}\cdot\mathbf{r}} \tag{4.24}$$

$$V(\mathbf{r}) = \sum_{\mathbf{G}} V_{\mathbf{G}} e^{j\mathbf{G}\cdot\mathbf{r}} \tag{4.25}$$

Substituting in Equation 4.1 yields

$$\beta \sum_{\mathbf{k}} Q_{\mathbf{k}} e^{j\mathbf{k}\cdot\mathbf{r}} = \frac{1}{2}\nabla_{\perp}^{2} \sum_{\mathbf{k}} Q_{\mathbf{k}} e^{j\mathbf{k}\cdot\mathbf{r}} + \sum_{\mathbf{G}} V_{\mathbf{G}} e^{j\mathbf{G}\cdot\mathbf{r}} \sum_{\mathbf{k}} Q_{\mathbf{k}} e^{j\mathbf{k}\cdot\mathbf{r}} \tag{4.26}$$

$$\sum_{\mathbf{k}} \beta Q_{\mathbf{k}} e^{j\mathbf{k}\cdot\mathbf{r}} = \frac{1}{2} \sum_{\mathbf{k}} Q_{\mathbf{k}} \left(-\mathbf{k}^{2}\right) e^{j\mathbf{k}\cdot\mathbf{r}} + \sum_{\mathbf{k}} \sum_{\mathbf{G}} Q_{\mathbf{k}} V_{\mathbf{G}} e^{j(\mathbf{k}+\mathbf{G})\cdot\mathbf{r}} \tag{4.27}$$

Let $\mathbf{k}' = \mathbf{k} + \mathbf{G}$ in the last summation and, given that $\mathbf{k}'$ is summed over the same space as $\mathbf{k}$, $\mathbf{k}'$ can be replaced with $\mathbf{k}$ in the summation:

$$\sum_{\mathbf{k}} \sum_{\mathbf{G}} Q_{\mathbf{k}} V_{\mathbf{G}} e^{j(\mathbf{k}+\mathbf{G})\cdot\mathbf{r}} = \sum_{\mathbf{k}'} \sum_{\mathbf{G}} Q_{\mathbf{k}'-\mathbf{G}} V_{\mathbf{G}} e^{j\mathbf{k}'\cdot\mathbf{r}} = \sum_{\mathbf{k}} \sum_{\mathbf{G}} Q_{\mathbf{k}-\mathbf{G}} V_{\mathbf{G}} e^{j\mathbf{k}\cdot\mathbf{r}} \tag{4.28}$$

The full equation is then:

$$\sum_{\mathbf{k}} \beta Q_{\mathbf{k}} e^{j\mathbf{k}\cdot\mathbf{r}} = \frac{1}{2} \sum_{\mathbf{k}} Q_{\mathbf{k}} \left(-\mathbf{k}^{2}\right) e^{j\mathbf{k}\cdot\mathbf{r}} + \sum_{\mathbf{k}} \sum_{\mathbf{G}} Q_{\mathbf{k}-\mathbf{G}} V_{\mathbf{G}} e^{j\mathbf{k}\cdot\mathbf{r}} \tag{4.29}$$

As the functions $e^{j\mathbf{k}\cdot\mathbf{r}}$ are orthogonal, the equation can be written for each $\mathbf{k}$:

$$\beta Q_{\mathbf{k}} = -\frac{1}{2}\mathbf{k}^{2} Q_{\mathbf{k}} + \sum_{\mathbf{G}} Q_{\mathbf{k}-\mathbf{G}} V_{\mathbf{G}} \tag{4.30}$$

These equations can be written in matrix form as $\beta Q = HQ$, for a finite number of values of $\mathbf{k}$, which allows to obtain an approximation using the smaller spatial frequencies. Similar to the finite differences method, this is also an eigenvalue problem.

4.3.1 Fourier Series Approximation

The Fourier series representation of $V(u,v)$ is presented in Equation 4.25. Coefficients for large enough $|\mathbf{G}|$ are typically negligible and, in such cases, it can be truncated. In normalized coordinates, described in Section 4.1, and using Equation 4.12, the truncated series representation is then

$$\begin{aligned} V(u,v) &= \sum_{g_u=-N_u}^{N_u} \sum_{g_v=-N_v}^{N_v} V_{g_u\mathbf{b}_1+g_v\mathbf{b}_2} e^{j(g_u\mathbf{b}_1+g_v\mathbf{b}_2)\cdot(u\mathbf{a}_1+v\mathbf{a}_2)} \\ V(u,v) &= \sum_{g_u=-N_u}^{N_u} \sum_{g_v=-N_v}^{N_v} V_{g_u,g_v} e^{j2\pi(g_u u+g_v v)} \end{aligned} \tag{4.31}$$

This is the DFT representation of $V(u,v)$, scaled by $(2N_u+1)(2N_v+1)$, for $u = \frac{n_u}{2N_u+1}$ and $v = \frac{n_v}{2N_v+1}$. Therefore, the DFT coefficients can be used as Fourier series coefficients, with proper scaling.

4.4 Lattice Analysis

A lattice analysis defines one or more potentials V for which Equation 4.1 should be solved, as well as the corresponding boundary conditions. It also defines the metrics that should be computed, for example, the integral form factor. Four types of lattice analyses were defined: periodic, finite, χ as a function of p_2, and χ as a function of p_2 and θ.

The periodic lattice analysis allows computing the solutions of the PDE for a specific periodic potential, using Bloch boundary conditions for different values of $\mathbf{k}$. The space to consider is a primitive cell. The outputs are the band structure and the wave functions ψ_n associated with each propagation constant $\beta_n(\mathbf{k})$. The $\beta_n(\mathbf{k})$ are sorted in descending order.

The finite lattice analysis computes the linear modes in a finite region, which is a parallelogram, using zero boundary conditions. The outputs are the values of β_n, sorted in descending order, the integral form factors χ_n, and the wave functions ψ_n.

The other two lattice analyses are both based on the finite one. They both output the form factors χ as a function of the intensity of the second lattice p_2 (assuming the intensity of the first lattice, p_1, is fixed), but one of them also sweeps through different values of the rotation angle θ. The outputs of these analyses can be used to reproduce the results in Figures 3.4 and 3.5, for example.

4.5 Testing

Some unit tests are implemented to ensure the results are valid. The most relevant tests consist of verifying that the result of the numerical methods verify the following properties:

- It is an approximate solution of the PDE in the space domain.
- The eigenvalues (i.e. propagation constants β) have a low relative error when increasing the number of discretization points.
- It is an approximate solution of the PDE in the spatial frequency domain (only for periodic potentials).
- The eigenvalues (i.e. propagation constants β) are invariant to the translation of the potential (only for periodic potentials).

These tests are also useful to better understand the limitations of the numerical eigenvalues solver, and adjust its parameters as needed.

4.6 Summary

This chapter describes the most relevant aspects of the designed methodology. It consists of a core algorithm that computes the solutions of the PDE (Equation 4.1) according to the specified potential and boundary conditions. The core algorithm is then integrated into higher-level algorithms that define the cases for which the PDE solutions should be computed, as well as the appropriate data processing and visualization steps. They ensure that the results are consistent and easier to obtain. Finally, to validate the correctness of the most important parts of the algorithm, some unit tests have been implemented.

The next three chapters present many examples computed using these algorithms, with detailed descriptions of the obtained results. Thus, the information that is provided in this chapter is complemented by those descriptions.

Chapter 5

Periodic Moiré Lattices

Periodic lattices, in particular, moiré lattices, do not exist in practice. They are, however, a very useful and simple model that allows to predict the behavior of very large crystalline structures. Additionally, as explored in [4], quasiperiodic structures can be approximated by periodic ones. Therefore, it is possible to obtain an approximation of the band structure of the quasiperiodic structure by choosing an appropriate periodic approximation. This chapter explores four different types of moiré lattices formed by the superimposition of a Bravais lattice and its rotated copy, namely: square, hexagonal, rectangular and centered rectangular. The periodicity conditions are discussed briefly, and some examples of periodic potentials are presented. These examples include the respective band structure and the magnitude of a wave function in the top band.

In the examples, the considered moiré potential is

$$V(u_1, v_1, u_2, v_2) = p_1 V'(u_1, v_1) + p_2 V'(u_2, v_2) \tag{5.1}$$

where u_1, v_1, u_2, v_2 are normalized coordinates, described in 4.1 and

$$V'(u, v) = \cos(2\pi u) + \cos(2\pi v) \tag{5.2}$$

is the potential representing a Bravais lattice.

The band structure is presented as $\mathbf{k}$ goes along the path

$$\Gamma \to M \to X \to \Gamma$$

which is defined according to the conventional primitive vectors of the reciprocal lattice: Γ corresponds to the origin, M to $\mathbf{b}_1$, and X to $\mathbf{b}_1 + \mathbf{b}_2$.

To obtain comparable results, the basis matrix A_1 (which defines the Bravais lattice) is normalized such that $|\det(A_1)| = \pi^2$, i.e. the area of the primitive cell is π^2. The rotated basis matrix is

$$A_2 = R^\theta A_1 \tag{5.3}$$

where R^θ represents an anticlockwise rotation matrix for angle θ. The space matrix A corresponds to a primitive cell. Thus, it depends on the chosen lattice. Additionally, $p_1 = 1$ and p_2 can vary. Finally, the PDE is solved using the finite differences method, with Bloch boundary conditions. The plane wave decomposition method was also used, mainly for comparison, and it yields very similar results, as expected.

5.1 Square

5.1.1 Periodicity Condition

First, to better visualize the concept of a square moiré lattice, Figure 5.1 presents a square lattice with its primitive lattice vectors $\mathbf{a}_1^{(1)}$ and $\mathbf{a}_2^{(1)}$, its rotated copy with vectors $\mathbf{a}_1^{(2)}$ and $\mathbf{a}_2^{(2)}$, and the resulting moiré lattice with vectors $\mathbf{a}_1$ and $\mathbf{a}_2$.

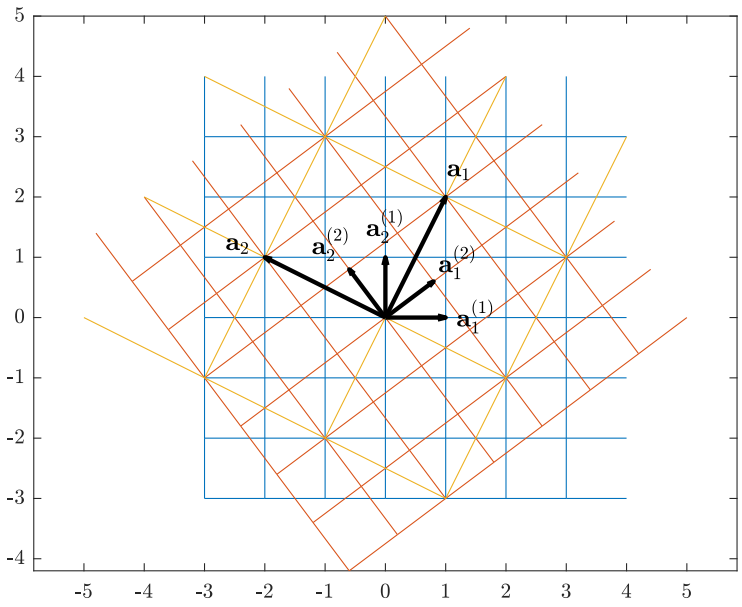

Figure 5.1: Square moiré lattice (yellow) as a superimposition of a square lattice (blue) and its rotated copy (orange).

Let L be the length of the primitive lattice vectors. Then, they can be expressed in complex numbers as $z_1 = L$ and $z_2 = Lj$, corresponding to $\mathbf{a}_1^{(1)}$ and $\mathbf{a}_2^{(1)}$, respectively. Additionally, the rotated lattice primitive vectors are $e^{j\theta}z_1$ and $e^{j\theta}z_2$, corresponding to $\mathbf{a}_1^{(2)}$ and $\mathbf{a}_2^{(2)}$, respectively. The moiré lattice vectors must belong to both lattices so, representing them as a complex number z_m, the periodicity condition is

$$\begin{aligned} z_m &= m_1 L + m_2 Lj = e^{j\theta}\left(m_3 L + m_4 Lj\right) \\ \frac{z_m}{L} &= m_1 + m_2 j \quad\;\; = e^{j\theta}\left(m_3 + m_4 j\right) \end{aligned} \tag{5.4}$$

where $m_1, m_2, m_3, m_4 \in \mathbb{Z}$ and $\theta \in [0, \pi[$. It can then be rewritten with respect to $e^{j\theta}$:

$$\begin{aligned} e^{j\theta} &= \frac{m_1 + m_2 j}{m_3 + m_4 j} \\ &= \frac{(m_1 + m_2 j)(m_3 - m_4 j)}{m_3^2 + m_4^2} \\ &= \frac{(m_1 m_3 + m_2 m_4) + (m_2 m_3 - m_1 m_4) j}{m_3^2 + m_4^2} \end{aligned} \tag{5.5}$$

Let

$$\begin{aligned} a &= m_1 m_3 + m_2 m_4 \\ b &= m_2 m_3 - m_1 m_4 \\ c &= m_3^2 + m_4^2 \end{aligned}$$

Then, Equation 5.5 becomes

$$e^{j\theta} = \frac{a + bj}{c} \tag{5.6}$$

where $a, b, c \in \mathbb{Z}$. The corresponding condition for the rotation angle θ is then

$$\tan(\theta) = \frac{b}{a} \tag{5.7}$$

and the magnitude condition is

$$a^2 + b^2 = c^2 \tag{5.8}$$

which is a Diophantine equation, i.e. an equation whose unknowns are integers. This particular equation corresponds to the Pythagorean theorem and its solutions are the Pythagorean triples [24].

Substituting in Equation 5.4 yields

$$m_1 + m_2 j = \left(\frac{a + bj}{c}\right)(m_3 + m_4 j)$$

which is equivalent to a system of linear Diophantine equations:

$$\begin{cases} cm_1 = am_3 - bm_4 \\ cm_2 = bm_3 + am_4 \end{cases} \tag{5.9}$$

Solving this system generates the moiré lattice vectors. Solving it for generic values of a, b, c is not trivial but, for concrete values, it may be done computationally.

However, for square moiré lattices, there is a shortcut that allows to compute the primitive lattice vectors. The solutions of Equation 5.8 are given by

$$a = k\left(n_1^2 - n_2^2\right) \qquad b = k(2n_1 n_2) \qquad c = k\left(n_1^2 + n_2^2\right) \tag{5.10}$$

where $k \in \mathbb{Z}$ and $n_1, n_2 \in \mathbb{Z}$, are coprime, and one of them is even. This condition ensures that a, b, c are pairwise coprime when $k = 1$. It is important to note that a and b may be exchanged and k is redundant in the equation (not in the solutions). Then, a and b uniquely determine θ and, given that c is the length of a lattice vector z_m, assigning $(m_1, m_2) = (n_1, n_2)$ ensures that z_m is a primitive lattice vector. Finally, due to symmetry, rotating any lattice vector by $\frac{\pi}{2}$ generates a lattice vector. Rewriting Equation 5.4 yields

$$j\frac{z_m}{L} = -m_2 + m_1 j = e^{j\theta}\left(-m_4 + m_3 j\right)$$

This lattice vector has the same length as the original one so, if the original vector is primitive, the generated one is primitive too. The four primitive vectors are then generated by

$$(m_1, m_2) = \pm(n_1, n_2) \tag{5.11}$$

$$(m_1, m_2) = \pm(-n_2, n_1) \tag{5.12}$$

These vectors are the vertices of a square and, as such, the moiré lattice is a square Bravais lattice.

5.1.2 Example

Based on [3], the example consists of a square moiré lattice with $L = \pi$ and $\tan(\theta) = \frac{3}{4}$, which corresponds to a solution of Equation 5.8 with $a = 4$, $b = 3$, and $c = 5$. This solution, according to the parameterization in Equation 5.10, is given by $n_1 = 1$ and $n_2 = 2$. The primitive lattice vectors are

$$\mathbf{a}_1 = L(n_1\hat{\mathbf{x}} + n_2\hat{\mathbf{y}}) = \pi\hat{\mathbf{x}} + 2\pi\hat{\mathbf{y}}$$
$$\mathbf{a}_2 = L(-n_2\hat{\mathbf{x}} + n_1\hat{\mathbf{y}}) = -2\pi\hat{\mathbf{x}} + \pi\hat{\mathbf{y}}$$

Different values of p_2 are compared in Figure 5.2: $p_2 = 0.1$ and $p_2 = 0.4$. In the first case, it is possible to observe that the bands are not flat, and the wave associated with the top band at $\mathbf{k} = \Gamma$ has a significant magnitude along the primitive cell. However, in the second case, the top band is flat, and the associated wave at $\mathbf{k} = \Gamma$ has a significant magnitude mainly in the center.

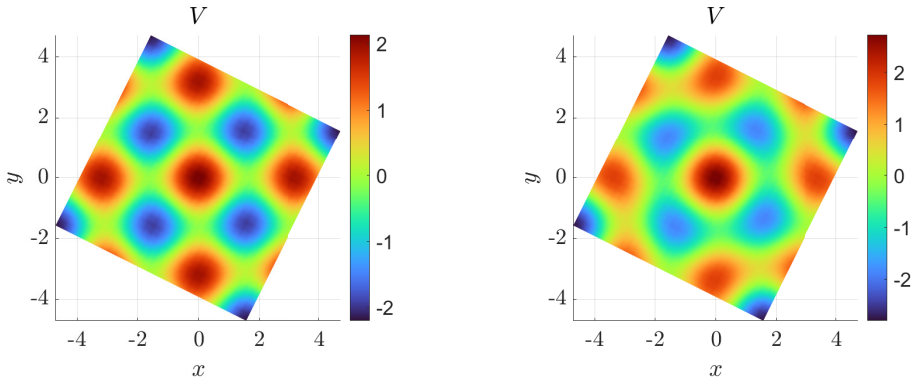

(a) Potential $V(x,y)$

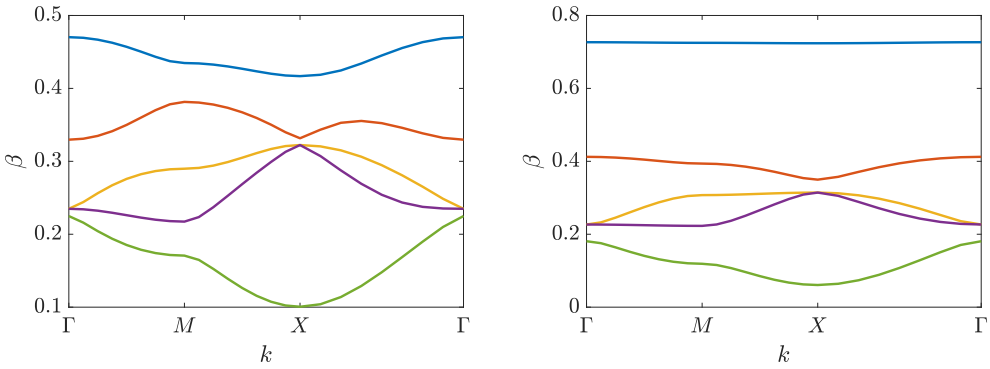

(b) Band structure

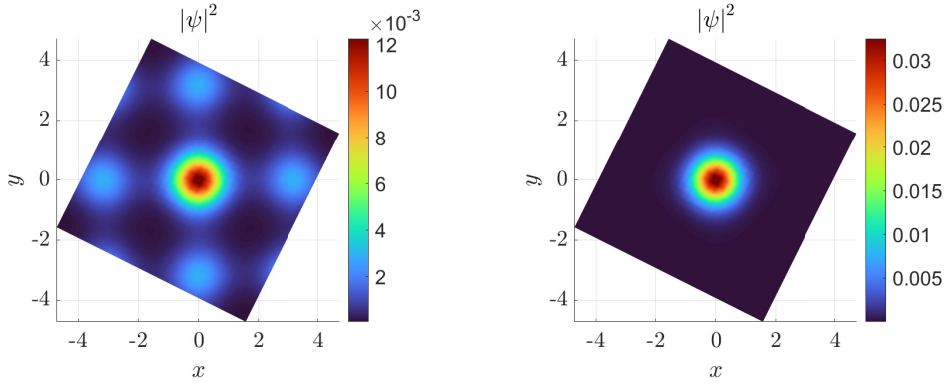

(c) Squared magnitude of the wave function ψ associated with the largest β_n at $\mathbf{k} = \Gamma$

Figure 5.2: Periodic square moiré lattices, with $\tan(\theta) = 3/4$. Different values of p_2 are compared: 0.1 (left) and 0.4 (right).

5.2 Hexagonal

5.2.1 Periodicity Condition

Similar to the square moiré lattice, Figure 5.3 illustrates a hexagonal moiré lattice.

Let L be the length of the primitive lattice vectors. Then, similar to the square lattice, they can

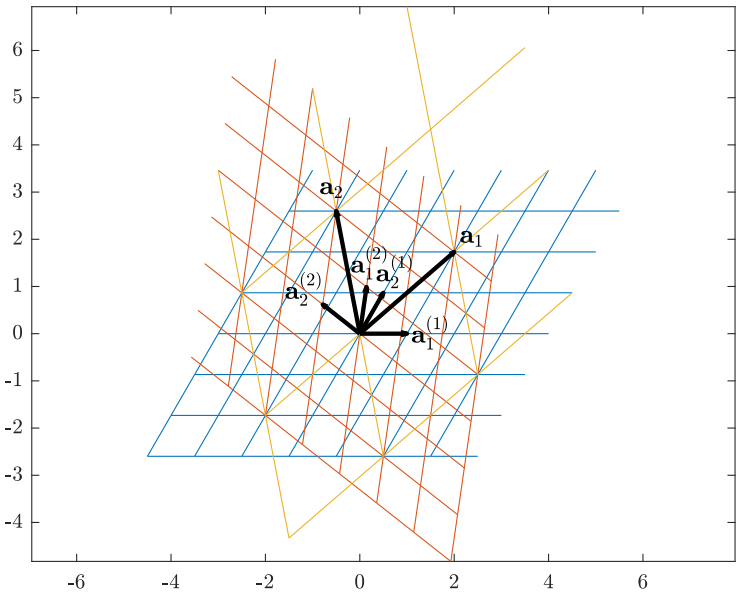

Figure 5.3: Hexagonal moiré lattice (yellow) as a superimposition of a hexagonal lattice (blue) and its rotated copy (orange).

be expressed in complex numbers as $z_1 = L$ and $z_2 = Le^{j\frac{\pi}{3}}$, and the periodicity condition is

$$\begin{aligned} z_m &= m_1 L + m_2 L e^{j\frac{\pi}{3}} &&= e^{j\theta}\left(m_3 L + m_4 L e^{j\frac{\pi}{3}}\right) \\ \frac{z_m}{L} &= m_1 + m_2 e^{j\frac{\pi}{3}} &&= e^{j\theta}\left(m_3 + m_4 e^{j\frac{\pi}{3}}\right) \end{aligned} \tag{5.13}$$

where $m_1, m_2, m_3, m_4 \in \mathbb{Z}$ and $\theta \in [0, \pi[$. It can then be rewritten with respect to $e^{j\theta}$:

$$\begin{aligned} e^{j\theta} &= \frac{m_1 + m_2 e^{j\frac{\pi}{3}}}{m_3 + m_4 e^{j\frac{\pi}{3}}} \\ &= \frac{\left(m_1 + m_2 e^{j\frac{\pi}{3}}\right)\left(m_3 + m_4 e^{-j\frac{\pi}{3}}\right)}{m_3^2 + m_3 m_4 + m_4^2} \\ &= \frac{(m_1 m_3 + m_2 m_4) + m_2 m_3 e^{j\frac{\pi}{3}} + m_1 m_4 e^{-j\frac{\pi}{3}}}{m_3^2 + m_3 m_4 + m_4^2} \\ &= \frac{(m_1 m_3 + m_2 m_4) + m_2 m_3 e^{j\frac{\pi}{3}} + m_1 m_4\left(1 - e^{j\frac{\pi}{3}}\right)}{m_3^2 + m_3 m_4 + m_4^2} \\ &= \frac{(m_1 m_3 + m_2 m_4 + m_1 m_4) + (m_2 m_3 - m_1 m_4) e^{j\frac{\pi}{3}}}{m_3^2 + m_3 m_4 + m_4^2} \end{aligned} \tag{5.14}$$

Let

$$\begin{aligned} a &= m_1 m_3 + m_2 m_4 + m_1 m_4 \\ b &= m_2 m_3 - m_1 m_4 \\ c &= m_3^2 + m_3 m_4 + m_4^2 \end{aligned}$$

Then, Equation 5.14 becomes

$$e^{j\theta} = \frac{a + b e^{j\frac{\pi}{3}}}{c} \tag{5.15}$$

where $a, b, c \in \mathbb{Z}$. It can also be written as

$$e^{j\theta} = \frac{a + \frac{b}{2} + \frac{\sqrt{3}}{2} b j}{c} \tag{5.16}$$

The corresponding condition for the rotation angle θ is then

$$\tan(\theta) = \sqrt{3} \frac{b}{2a + b} \tag{5.17}$$

and the magnitude condition is

$$a^2 + ab + b^2 = c^2 \tag{5.18}$$

which is a Diophantine equation.

Substituting in Equation 5.13 yields

$$\begin{aligned} m_1 + m_2 e^{j\frac{\pi}{3}} &= \left(\frac{a + b e^{j\frac{\pi}{3}}}{c} \right) \left(m_3 + m_4 e^{j\frac{\pi}{3}} \right) \\ c \left(m_1 + m_2 e^{j\frac{\pi}{3}} \right) &= a m_3 + (a m_4 + b m_3) e^{j\frac{\pi}{3}} + b m_4 e^{j\frac{2\pi}{3}} \\ c \left(m_1 + m_2 e^{j\frac{\pi}{3}} \right) &= a m_3 + (a m_4 + b m_3) e^{j\frac{\pi}{3}} + b m_4 \left(e^{j\frac{\pi}{3}} - 1 \right) \\ c \left(m_1 + m_2 e^{j\frac{\pi}{3}} \right) &= a m_3 - b m_4 + (a m_4 + b m_3 + b m_4) e^{j\frac{\pi}{3}} \end{aligned}$$

which is equivalent to a system of linear Diophantine equations:

$$\begin{cases} c m_1 = a m_3 - b m_4 \\ c m_2 = b m_3 + (a + b) m_4 \end{cases} \tag{5.19}$$

This system is similar to the one found for the square lattice, i.e. it generates all moiré lattice vectors and is hard to solve for generic values of a, b, c.

Determining the primitive lattice vectors is not easy, unlike square moiré lattices. However, given a primitive lattice vector, the other primitive vectors can be obtained similarly, but rotating by $\frac{\pi}{3}$ instead of $\frac{\pi}{2}$. Rewriting Equation 5.13 yields

$$e^{j\frac{\pi}{3}} \frac{z_m}{L} = -m_2 + (m_1 + m_2) e^{j\frac{\pi}{3}} = e^{j\theta} \left(-m_4 + (m_3 + m_4) e^{j\frac{\pi}{3}} \right)$$

This lattice vector has the same length as the original one so, if the original vector is primitive, the generated one is primitive too. The six primitive vectors are then generated by

$$(m_1, m_2) = \pm(n_1, n_2) \tag{5.20}$$

$$(m_1, m_2) = \pm(-n_2, n_1 + n_2) \tag{5.21}$$

$$(m_1, m_2) = \pm(-n_1 - n_2, n_1) \tag{5.22}$$

for a given primitive vector with $(m_1, m_2) = (n_1, n_2)$.

These vectors are the vertices of a hexagon and, as such, the moiré lattice is a hexagonal Bravais lattice.

5.2.2 Example

The example consists of a hexagonal moiré lattice with $\tan(\theta) = 4\sqrt{3}$, which corresponds to a solution of Equation 5.18 with $a = 3$, $b = -8$, and $c = 7$. Different values of p_2 are compared in Figure 5.4: $p_2 = 0.1$ and $p_2 = 0.4$. In the first case, it is possible to observe that the bands are not flat, and the wave associated with the top band at $\mathbf{k} = \Gamma$ has a significant magnitude along the primitive cell. However, in the second case, the top band is almost flat, and the associated wave at $\mathbf{k} = \Gamma$ has a significant magnitude mainly in the center.

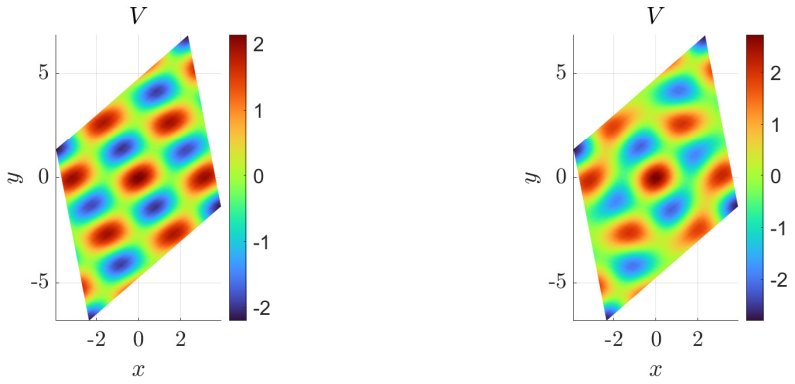

(a) Potential $V(x,y)$

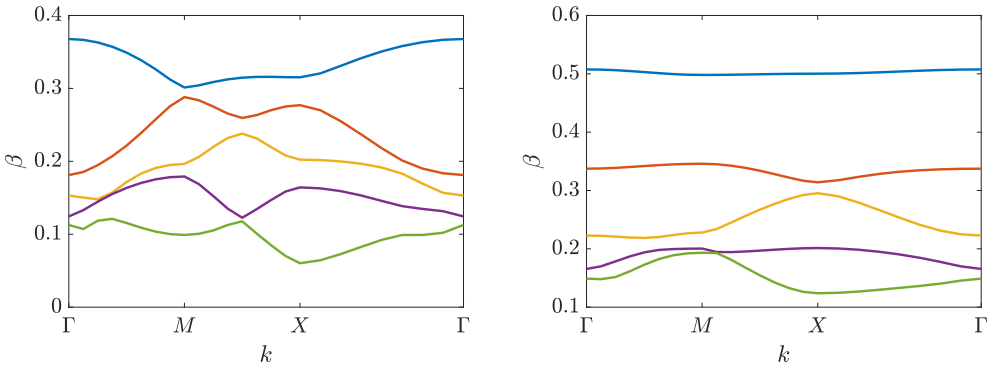

(b) Band structure

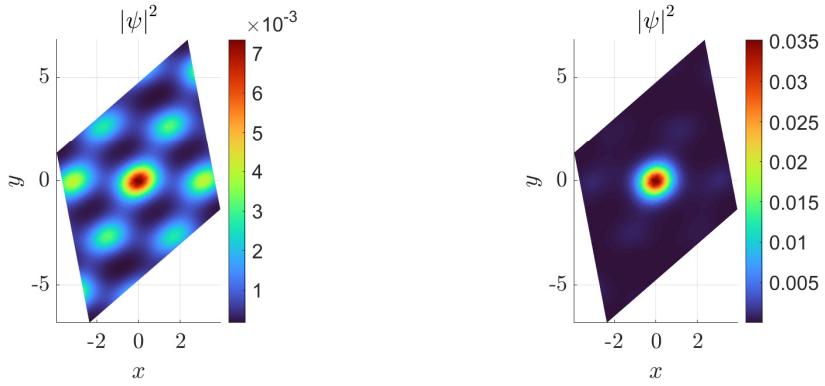

(c) Squared magnitude of the wave function ψ associated with the largest β_n at $\mathbf{k} = \Gamma$

Figure 5.4: Periodic hexagonal moiré lattice, with $\tan(\theta) = 4\sqrt{3}$. Different values of p_2 are compared: 0.1 (left) and 0.4 (right).

5.3 Rectangular

5.3.1 Periodicity Condition

Similar to the square moiré lattice, Figure 5.5 illustrates a rectangular moiré lattice.

Let L_1 and L_2 be the lengths of the primitive lattice vectors and $\alpha = \frac{L_2}{L_1}$ their ratio. Then, similar to the square lattice, they can be expressed in complex numbers as $z_1 = L_1$ and $z_2 = L_2 j$,

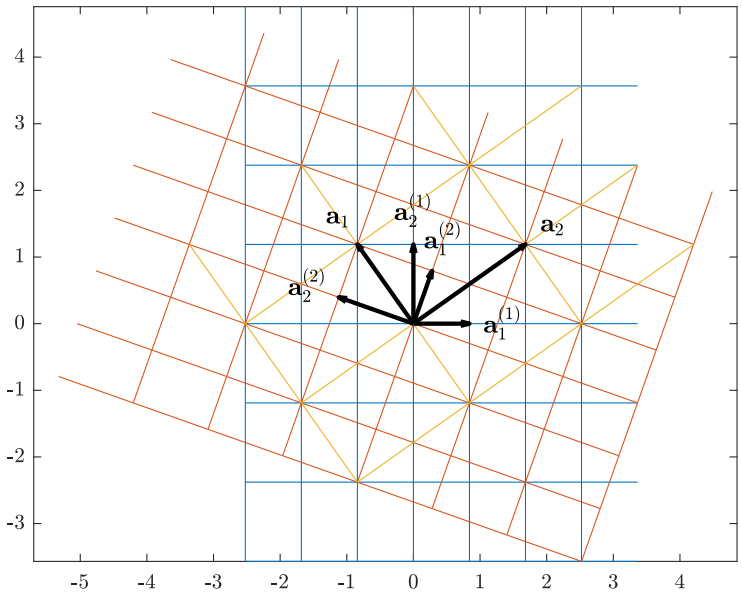

Figure 5.5: Rectangular moiré lattice (yellow) as a superimposition of a rectangular lattice (blue) and its rotated copy (orange).

and the periodicity condition is

$$\begin{aligned} z_m &= m_1 L_1 + m_2 L_2 j = e^{j\theta}\left(m_3 L_1 + m_4 L_2 j\right) \\ \frac{z_m}{L_1} &= m_1 + \alpha m_2 j \quad\;\; = e^{j\theta}\left(m_3 + \alpha m_4 j\right) \end{aligned} \tag{5.23}$$

where $m_1, m_2, m_3, m_4 \in \mathbb{Z}$ and $\theta \in [0, \pi[$.

Compared to the previous lattices, a new degree of freedom was introduced, α. The magnitude condition corresponding to Equation 5.23 is

$$m_1^2 + \alpha^2 m_2^2 = m_3^2 + \alpha^2 m_4^2$$

Rewriting this equation yields two overlapping conditions for α^2:

$$\begin{gathered} \left(m_1^2 - m_3^2\right) = \alpha^2\left(m_4^2 - m_2^2\right) \\ \left(\left(m_1^2 = m_3^2\right) \wedge \left(m_2^2 = m_4^2\right)\right) \vee \left(\alpha^2 = \frac{m_1^2 - m_3^2}{m_4^2 - m_2^2}\right) \end{gathered} \tag{5.24}$$

To simplify, they will be referred to as free and rational conditions, respectively, according to the restriction they imply on α^2. They are studied in more detail in Sections 5.3.1.1 and 5.3.1.2.

5.3.1.1 Free Condition

The free condition is

$$\begin{cases} m_3^2 = m_1^2 \\ m_4^2 = m_2^2 \end{cases} \quad \begin{cases} m_3 = \pm m_1 \\ m_4 = \pm m_2 \end{cases}$$

The case $(m_3, m_4) = \pm(m_1, m_2)$ is degenerate, as it can be easily seen that the resulting θ will be 0. However, the remaining case, $(m_3, m_4) = \pm(-m_1, m_2)$, is non-trivial.

To simplify, let $m_1 = n_1$ and $m_2 = n_2$, where $n_1, n_2 \in \mathbb{Z}$. Substituting the non-degenerate case in Equation 5.23 and developing yields the condition for θ:

$$\begin{aligned} n_1 + \alpha n_2 j &= e^{j\theta}(-n_1 + \alpha n_2 j) \\ e^{j\theta} &= \frac{n_1 + \alpha n_2 j}{-n_1 + \alpha n_2 j} \\ e^{j\theta} &= \frac{(n_1 + \alpha n_2 j)(-n_1 - \alpha n_2 j)}{n_1^2 + (\alpha n_2)^2} \\ e^{j\theta} &= -\frac{\left(n_1^2 - (\alpha n_2)^2\right) + 2\alpha n_1 n_2 j}{n_1^2 + (\alpha n_2)^2} \qquad (5.25) \\ \tan(\theta) &= \frac{2\alpha n_1 n_2}{n_1^2 - (\alpha n_2)^2} \qquad (5.26) \end{aligned}$$

Finally, it is relevant to note that, if α^2 is not rational, this is the only primitive lattice vector. Thus, this is a degenerate one-dimensional lattice, with primitive vectors generated by

$$(m_1, m_2) = \pm(n_1, n_2) \qquad (5.27)$$

5.3.1.2 Rational Condition

The rational condition is

$$\alpha^2 = \frac{m_1^2 - m_3^2}{m_4^2 - m_2^2} \qquad (5.28)$$

It can also be written as

$$\alpha^2 = \frac{B}{A} \qquad (5.29)$$

where $A, B \in \mathbb{Z}$ are coprime. Additionally, Equation 5.23 can be written as

$$\sqrt{A}\frac{z_m}{L_1} = m_1\sqrt{A} + m_2\sqrt{B}j = e^{j\theta}\left(m_3\sqrt{A} + m_4\sqrt{B}j\right) \qquad (5.30)$$

It can then be rewritten with respect to $e^{j\theta}$:

$$\begin{aligned} e^{j\theta} &= \frac{m_1\sqrt{A}+m_2\sqrt{B}j}{m_3\sqrt{A}+m_4\sqrt{B}j} \\ &= \frac{\left(m_1\sqrt{A}+m_2\sqrt{B}j\right)\left(m_3\sqrt{A}-m_4\sqrt{B}j\right)}{Am_3^2+Bm_4^2} \\ &= \frac{(Am_1m_3+Bm_2m_4)+\sqrt{AB}\,(m_2m_3-m_1m_4)\,j}{Am_3^2+Bm_4^2} \end{aligned} \tag{5.31}$$

Let

$$\begin{aligned} a &= Am_1m_3+Bm_2m_4 \\ b &= m_2m_3-m_1m_4 \\ c &= Am_3^2+Bm_4^2 \end{aligned}$$

Then, Equation 5.31 becomes

$$e^{j\theta} = \frac{a+\sqrt{AB}bj}{c} \tag{5.32}$$

where $a,b,c \in \mathbb{Z}$. The corresponding condition for the rotation angle θ is then

$$\tan(\theta) = \sqrt{AB}\frac{b}{a} \tag{5.33}$$

and the magnitude condition is

$$a^2+ABb^2 = c^2 \tag{5.34}$$

which is a Diophantine equation.

Substituting in Equation 5.30 yields

$$\begin{aligned} m_1\sqrt{A}+m_2\sqrt{B}j &= \left(\frac{a+\sqrt{AB}bj}{c}\right)\left(m_3\sqrt{A}+m_4\sqrt{B}j\right) \\ c\left(\sqrt{A}m_1+\sqrt{B}m_2j\right) &= \left(a\sqrt{A}m_3-b\sqrt{A}Bm_4\right)+\left(bA\sqrt{B}m_3+a\sqrt{B}m_4\right)j \end{aligned}$$

which is equivalent to a system of linear Diophantine equations:

$$\begin{cases} cm_1 = am_3-bBm_4 \\ cm_2 = bAm_3+am_4 \end{cases} \tag{5.35}$$

It generates all lattice vectors. Compared to the square and hexagonal linear systems, this one is even harder to solve generically due to the additional constants A,B.

5.3.2 Example

The example consists of a rectangular moiré lattice with $\alpha^2 = 2$ and $\tan(\theta) = 2\sqrt{2}$, which corresponds to a solution of Equation 5.34 with $a = 1$, $b = 2$, and $c = 3$. Different values of p_2 are compared in Figure 5.6: $p_2 = 0.1$ and $p_2 = 0.4$. In the first case, it is possible to observe that the bands are not flat, although they are flatter than in the previous cases, and the wave associated with the top band at $\mathbf{k} = \Gamma$ has a significant magnitude along the primitive cell. However, in the second case, the top band is flat, and the associated wave at $\mathbf{k} = \Gamma$ has a significant magnitude mainly in the center. Also, the following two bands are almost flat.

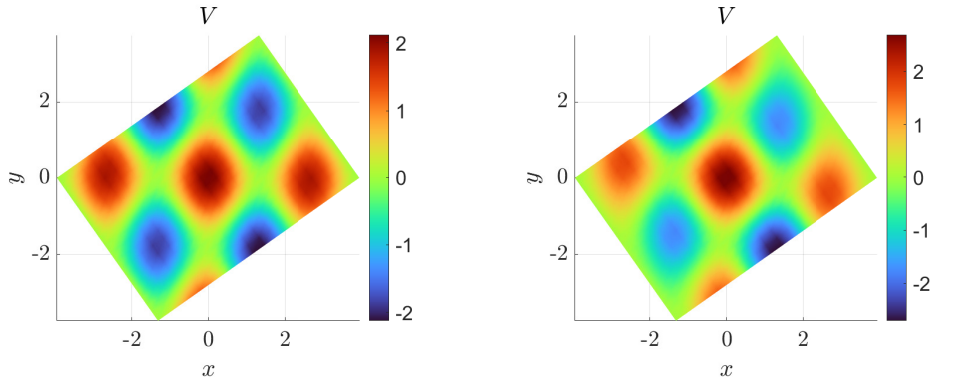

(a) Potential $V(x,y)$

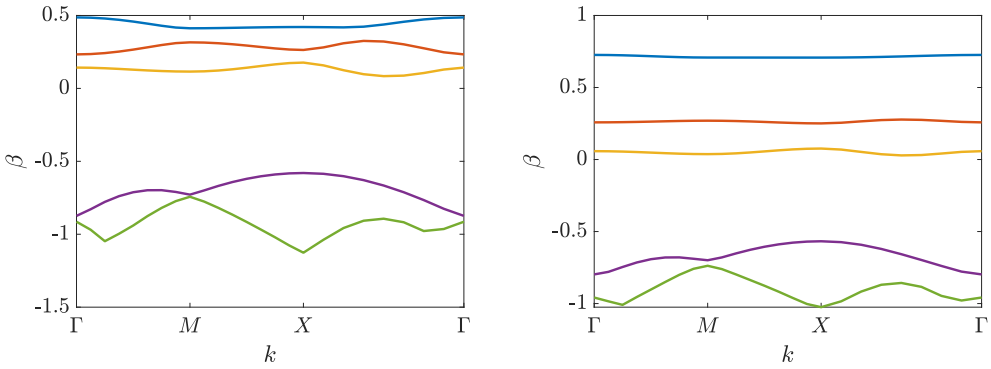

(b) Band structure

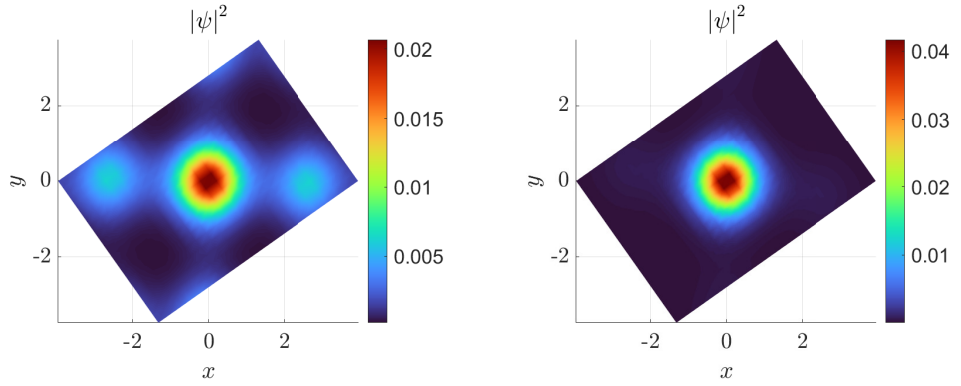

(c) Squared magnitude of the wave function ψ associated with the largest β_n at $\mathbf{k} = \Gamma$

Figure 5.6: Periodic rectangular moiré lattice, with $\alpha = \sqrt{2}$, $\tan(\theta) = 2\sqrt{2}$. Different values of p_2 are compared: 0.1 (left) and 0.4 (right).

5.4 Centered Rectangular

5.4.1 Periodicity Condition

Similar to the square moiré lattice, Figure 5.7 illustrates a centered rectangular moiré lattice.

Let L be the length of the primitive lattice vectors, and φ the angle between them. Then, similar to the square lattice, they can be expressed in complex numbers as $z_1 = L$ and $z_2 = Le^{j\varphi}$,

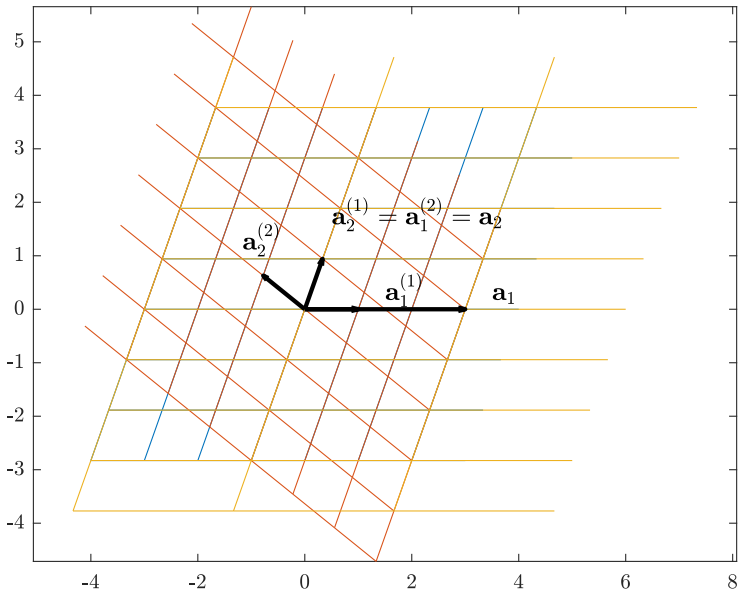

Figure 5.7: Centered rectangular moiré lattice (yellow) as a superimposition of a centered rectangular lattice (blue) and its rotated copy (orange).

and the periodicity condition is

$$\begin{aligned} z_m &= m_1 L + m_2 L e^{j\varphi} = e^{j\theta}\left(m_3 L + m_4 L e^{j\varphi}\right) \\ \frac{z_m}{L} &= m_1 + m_2 e^{j\varphi} \quad = e^{j\theta}\left(m_3 + m_4 e^{j\varphi}\right) \end{aligned} \tag{5.36}$$

where $m_1, m_2, m_3, m_4 \in \mathbb{Z}$ and $\theta \in [0, \pi[$.

Similarly to the rectangular lattice, a new degree of freedom was introduced, φ. The magnitude condition corresponding to Equation 5.36 is

$$m_1^2 + 2\cos(\varphi) m_1 m_2 + m_2^2 = m_3^2 + 2\cos(\varphi) m_3 m_4 + m_4^2$$

Rewriting this equation yields two overlapping conditions for $\cos(\varphi)$:

$$\begin{aligned} 2\cos(\varphi)(m_1 m_2 - m_3 m_4) &= \left(m_3^2 + m_4^2\right) - \left(m_1^2 + m_2^2\right) \\ \left((m_1 m_2 = m_3 m_4) \wedge \left(m_1^2 + m_2^2 = m_3^2 + m_4^2\right)\right) \vee &\left(\cos(\varphi) = \frac{\left(m_3^2 + m_4^2\right) - \left(m_1^2 + m_2^2\right)}{m_1 m_2 - m_3 m_4}\right) \end{aligned} \tag{5.37}$$

To simplify, they will be referred to as free and rational conditions, respectively, according to the restriction they imply on $\cos(\varphi)$. They are studied in more detail in Sections 5.3.1.1 and 5.3.1.2.

5.4.1.1 Free Condition

The free condition is

$$\begin{cases} m_1 m_2 = m_3 m_4 \\ m_1^2 + m_2^2 = m_3^2 + m_4^2 \end{cases}$$
$$\begin{cases} m_1^2 + 2m_1 m_2 + m_2^2 = m_3^2 + 2m_3 m_4 + m_4^2 \\ m_1^2 - 2m_1 m_2 + m_2^2 = m_3^2 - 2m_3 m_4 + m_4^2 \end{cases}$$
$$\begin{cases} (m_1 + m_2)^2 = (m_3 + m_4)^2 \\ (m_1 - m_2)^2 = (m_3 - m_4)^2 \end{cases}$$

This condition has four possible solutions:

$$(m_3, m_4) = \pm (m_1, m_2)$$
$$(m_3, m_4) = \pm (m_2, m_1)$$

The case $(m_3, m_4) = \pm (m_1, m_2)$ is degenerate, as it can be easily seen that the resulting θ will be 0. However, the remaining case, $(m_3, m_4) = \pm (m_2, m_1)$, is non-trivial.

To simplify, let $m_1 = n_1$ and $m_2 = n_2$, where $n_1, n_2 \in \mathbb{Z}$. Substituting the non-degenerate case in Equation 5.36 and developing yields the condition for θ:

$$\begin{aligned} n_1 + n_2 e^{j\varphi} &= e^{j\theta} \left(n_2 + n_1 e^{j\varphi} \right) \\ e^{j\theta} &= \frac{n_1 + n_2 e^{j\varphi}}{n_2 + n_1 e^{j\varphi}} \\ e^{j\theta} &= \frac{\left(n_1 + n_2 e^{j\varphi} \right) \left(n_2 + n_1 e^{-j\varphi} \right)}{n_1^2 + 2\cos(\varphi) n_1 n_2 + n_2^2} \\ e^{j\theta} &= \frac{\left(\left(n_1^2 + n_2^2 \right) \cos(\varphi) + 2 n_1 n_2 \right) + \left(n_2^2 - n_1^2 \right) \sin(\varphi) j}{n_1^2 + 2\cos(\varphi) n_1 n_2 + n_2^2} \end{aligned} \tag{5.38}$$

$$\tan(\theta) = \frac{\left(n_2^2 - n_1^2 \right) \sin(\varphi)}{\left(n_1^2 + n_2^2 \right) \cos(\varphi) + 2 n_1 n_2} \tag{5.39}$$

Finally, it is relevant to note that, if $\cos(\varphi)$ is not rational, this is the only primitive lattice vector. Thus, this is a degenerate one-dimensional lattice, with primitive vectors generated by

$$(m_1, m_2) = \pm (n_1, n_2) \tag{5.40}$$

5.4.1.2 Rational Condition

The rational condition is

$$\cos(\varphi) = \frac{\left(m_3^2 + m_4^2\right) - \left(m_1^2 + m_2^2\right)}{m_1 m_2 - m_3 m_4} \tag{5.41}$$

It can also be written as

$$\cos(\varphi) = \frac{B}{A} \tag{5.42}$$

where $A, B \in \mathbb{Z}$ are coprime and $A^2 > B^2$. Additionally, Equation 5.36 can be written with respect to $e^{j\theta}$:

$$\begin{aligned}
e^{j\theta} &= \frac{m_1 + m_2 e^{j\varphi}}{m_3 + m_4 e^{j\varphi}} \\
&= \frac{\left(m_1 + m_2 e^{j\varphi}\right)\left(m_3 + m_4 e^{-j\varphi}\right)}{m_3^2 + 2\cos(\varphi) m_3 m_4 + m_4^2} \\
&= \frac{m_1 m_3 + m_2 m_4 + m_2 m_3 e^{j\varphi} + m_1 m_4 e^{-j\varphi}}{m_3^2 + 2\cos(\varphi) m_3 m_4 + m_4^2} \\
&= \frac{m_1 m_3 + m_2 m_4 + 2\cos(\varphi)\left(m_2 m_3 + m_1 m_4\right) + 2\sin(\varphi)\left(m_2 m_3 - m_1 m_4\right) j}{m_3^2 + 2\cos(\varphi) m_3 m_4 + m_4^2} \\
&= \frac{m_1 m_3 + m_2 m_4 + 2\frac{B}{A}\left(m_2 m_3 + m_1 m_4\right) + 2\sqrt{1 - \left(\frac{B}{A}\right)^2}\left(m_2 m_3 - m_1 m_4\right) j}{m_3^2 + 2\frac{B}{A} m_3 m_4 + m_4^2} \\
&= \frac{A\left(m_1 m_3 + m_2 m_4\right) + 2B\left(m_2 m_3 + m_1 m_4\right) + 2\sqrt{A^2 - B^2}\left(m_2 m_3 - m_1 m_4\right) j}{A m_3^2 + 2B m_3 m_4 + A m_4^2}
\end{aligned} \tag{5.43}$$

Let

$$\begin{aligned}
a &= A\left(m_1 m_3 + m_2 m_4\right) + 2B\left(m_2 m_3 + m_1 m_4\right) \\
b &= 2\left(m_2 m_3 - m_1 m_4\right) \\
c &= A m_3^2 + 2B m_3 m_4 + A m_4^2
\end{aligned}$$

Then, Equation 5.43 becomes

$$e^{j\theta} = \frac{a + \sqrt{A^2 - B^2} b j}{c} \tag{5.44}$$

where $a, b, c \in \mathbb{Z}$. The corresponding condition for the rotation angle θ is then

$$\tan(\theta) = \sqrt{A^2 - B^2}\frac{b}{a} \tag{5.45}$$

and the magnitude condition is

$$a^2 + \left(A^2 - B^2\right) b^2 = c^2 \tag{5.46}$$

which is a Diophantine equation.

Substituting in Equation 5.36 yields

$$
\begin{aligned}
m_1 + m_2 e^{j\varphi} &= \left(\frac{a + \sqrt{A^2 - B^2}bj}{c} \right) \left(m_3 + m_4 e^{j\varphi} \right) \\
c\left(Am_1 + Bm_2 + \sqrt{A^2 - B^2}m_2 j \right) &= \left(\frac{a + \sqrt{A^2 - B^2}bj}{c} \right) \left(Am_3 + Bm_4 + \sqrt{A^2 - B^2}m_4 j \right) \\
c\left(Am_1 + Bm_2 + \sqrt{A^2 - B^2}m_2 j \right) &= a\left(Am_3 + Bm_4 \right) - b\left(A^2 - B^2 \right) m_4 \\
&\quad + \sqrt{A^2 - B^2}\left(b\left(Am_3 + Bm_4 \right) + am_4 \right) j
\end{aligned}
$$

which is equivalent to a system of linear Diophantine equations:

$$
\begin{cases}
cAm_1 + cBm_2 = aAm_3 + \left(aB - b\left(A^2 - B^2 \right) \right) m_4 \\
cm_2 = bAm_3 + \left(bB + a \right) m_4
\end{cases}
$$

$$
\begin{cases}
cAm_1 = A\left(a - bB \right) m_3 - bA^2 m_4 \\
cm_2 = bAm_3 + \left(bB + a \right) m_4
\end{cases}
$$

$$
\begin{cases}
cm_1 = \left(a - bB \right) m_3 - bAm_4 \\
cm_2 = bAm_3 + \left(bB + a \right) m_4
\end{cases}
\tag{5.47}
$$

Similar to other lattices, all moiré lattice vectors are generated by this linear system, and it is harder to solve generically than for the square or hexagonal cases due to constants A, B.

5.4.2 Example

The example consists of a centered rectangular moiré lattice with $\cos(\varphi) = 1/3$ and $\tan(\theta) = 2\sqrt{2}$, which corresponds to a solution of Equation 5.46 with $a = 1$, $b = 1$, and $c = 3$. Different values of p_2 are compared in Figure 5.8: $p_2 = 0.1$ and $p_2 = 0.4$. In the first case, it is possible to observe that the bands are not flat, and the wave associated with the top band at $\mathbf{k} = \Gamma$ has a significant magnitude along the primitive cell. In the second case, the top band is flatter, but still not flat, and the associated wave at $\mathbf{k} = \Gamma$ has a significant magnitude mainly in the center.

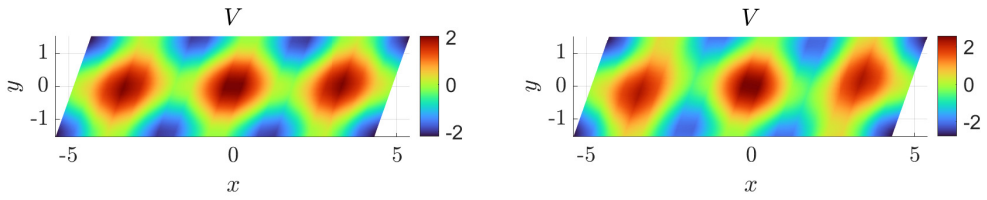

(a) Potential $V(x,y)$

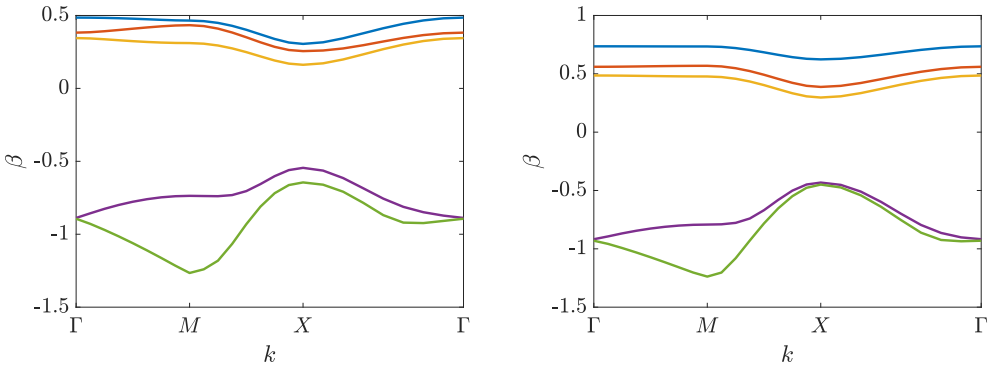

(b) Band structure

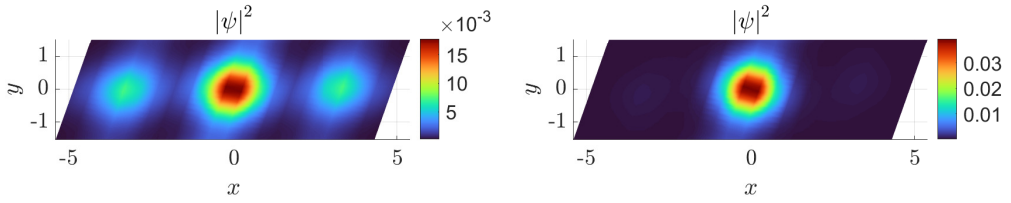

(c) Squared magnitude of the wave function ψ associated with the largest β_n at $\mathbf{k} = \Gamma$

Figure 5.8: Periodic centered rectangular moiré lattice, with $\cos(\varphi) = 1/3$ and $\tan(\theta) = 2\sqrt{2}$. Different values of p_2 are compared: 0.1 (left) and 0.4 (right).

5.5 Summary

This chapter presents the moiré lattices that were studied in this work: square, hexagonal, rectangular, and centered rectangular. For each of these lattices, the periodicity condition is obtained and a representative example of Bloch wave propagation is shown. It is relevant to note that the periodicity conditions are all given by a homogeneous degree two Diophantine equation. However, for rectangular and centered rectangular lattices, an additional condition is imposed on the

respective lattice parameter. The chosen solution determines the possible values for the relative rotation angle between the sublattices. Furthermore, it can be used to compute the coefficients of a system of linear Diophantine equations, whose solutions are all moiré lattice vectors. Finally, the examples illustrate Bloch wave propagation in a primitive cell, for a potential supported by each moiré lattice. The band structure and the wave profile for the top band with $\mathbf{k} = \Gamma$ are shown, and it is possible to observe that the flatness of the bands is related to the distribution of the magnitude of the wave, as stated in the literature.

The next chapter introduces more realistic potentials, considering that they are not infinite, by imposing a zero boundary condition in a defined region.

Chapter 6

Finite Moiré Lattices

The periodic lattices discussed in Chapter 5 are infinite. In practice, they do not exist, but truncating them to a finite area is possible. This area can be very large when compared to the primitive cell of the lattice and, in that case, the periodic model is a good approximation for most of the considered area. However, computing the PDE solutions in this finite area is very expensive computationally. To overcome this problem, smaller areas can be used, and the obtained approximations are reasonable.

Following a similar methodology as [3, 4], this chapter presents examples of periodic, aperiodic and, when possible, one-dimensional periodic moiré potentials based on square, hexagonal, rectangular, and centered rectangular Bravais lattices.

The considered moiré potential is the same as the previous chapter, given by Equation 5.1. The space matrix is

$$A = LI \tag{6.1}$$

where I is the 2×2 identity matrix, and L is the length of the side of the square defining the region. In this chapter, the value of L is 20π, while in [3] it is 40π, but the results can be scaled in most cases. As in the previous chapter, $p_1 = 1$, while p_2 can vary. Finally, the PDE is solved using the finite differences method, with zero boundary conditions.

6.1 Square

Square moiré lattices are extensively covered in the literature and have a relatively simple structure. As stated in [3], wave localization cannot occur on periodic potentials, in particular, potentials supported by a periodic square moiré lattice. This result is reproduced, with $\tan(\theta) = 3/4$ and $p_2 = 0.4$, in Figure 6.1, where the integral form factor, defined in 3.13, $\chi \approx 0.09$ and the magnitude of the wave function has periodic peaks along the considered region. An example of wave localization is also shown, for an aperiodic moiré lattice with $\tan(\theta) = \sqrt{3}$.

For the aperiodic lattice, wave localization depends on p_1 and p_2. In this example, two values of p_2 were considered: 0.1 and 0.4. Figure 6.2 presents an example of wave delocalization, for $p_2 = 0.1$, and localization, for $p_2 = 0.4$, corresponding to $\chi \approx 0.04$ and $\chi \approx 0.55$, respectively.

An overview of the localization-delocalization transition for these two examples can be analyzed in Figure 6.3. While the periodic potential is poorly localized for all p_2 in the considered interval, the aperiodic potential becomes localized at $p_2^{\mathrm{LDT}} \approx 0.14$. Finally, a global picture of χ as a function of θ and p_2 is presented in Figure 6.4, where it is possible to observe that p_2^{LDT} does not depend very strongly on θ.

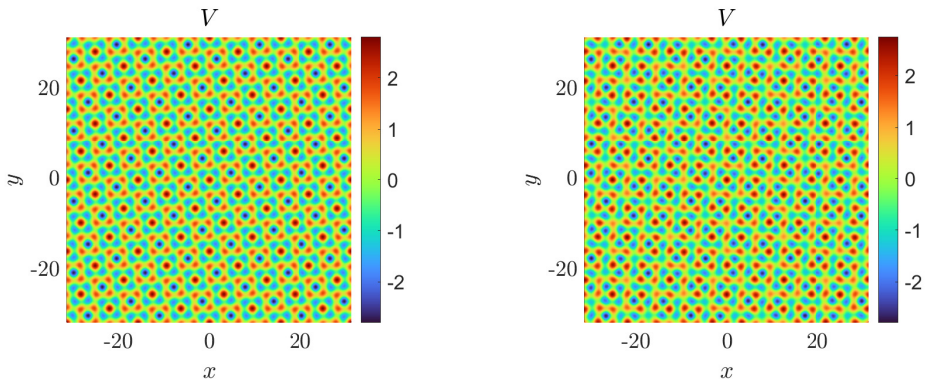

(a) Potential $V(x,y)$

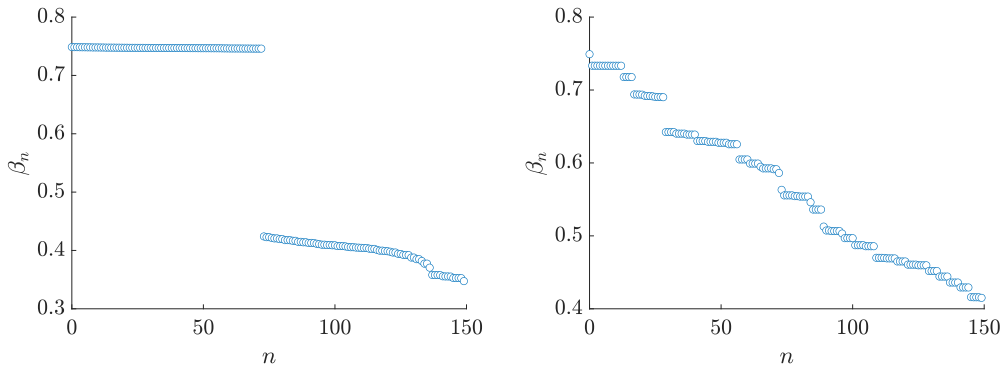

(b) Propagation constants β_n, in descending order

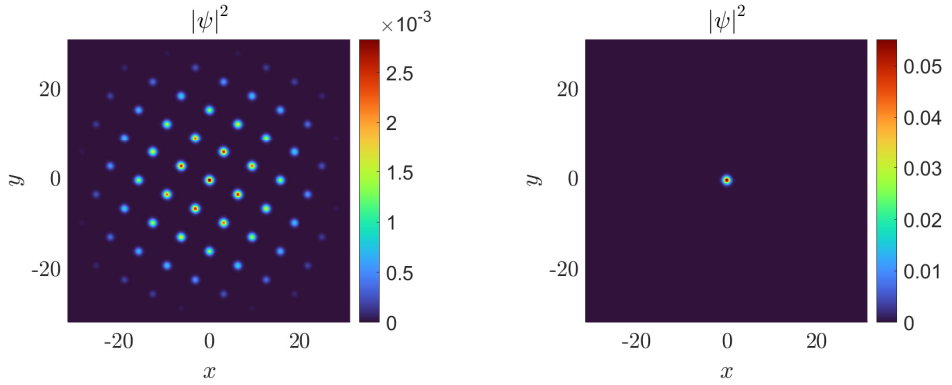

(c) Squared magnitude of the wave function ψ associated with the largest β_n

Figure 6.1: Finite square moiré lattice, with $p_2 = 0.4$. For the periodic lattice (left), $\tan(\theta) = 3/4$. For the aperiodic lattice (right), $\tan(\theta) = \sqrt{3}$.

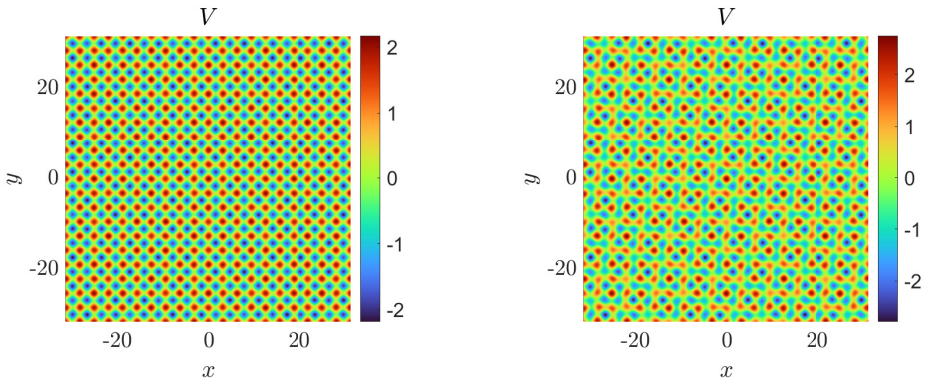

(a) Potential $V(x,y)$

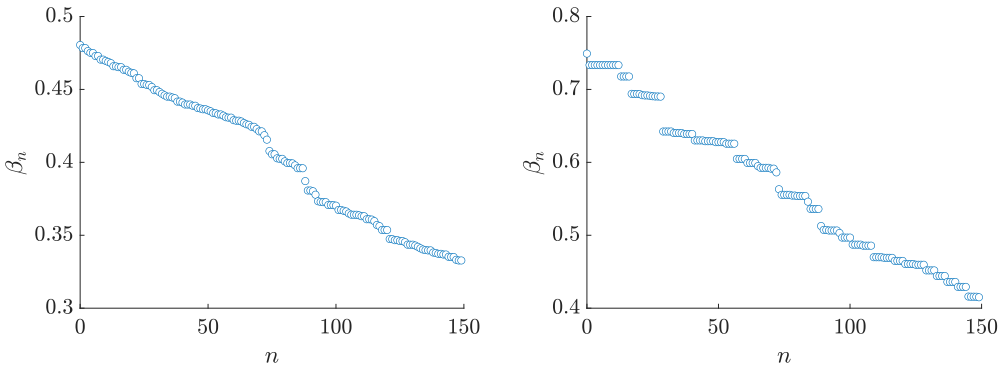

(b) Propagation constants β_n, in descending order

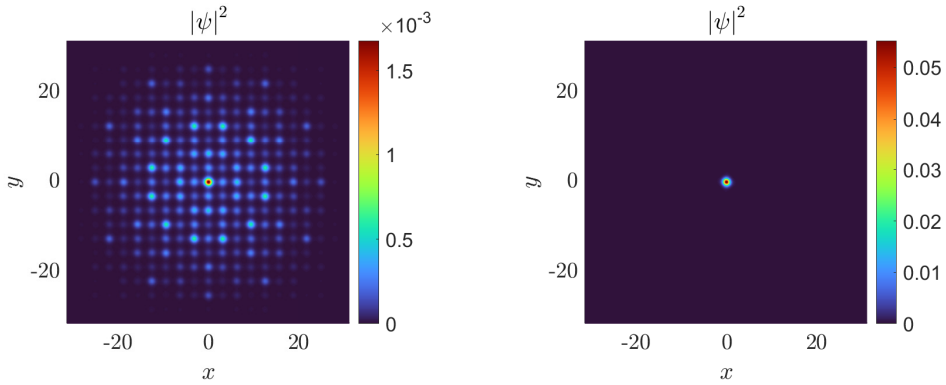

(c) Squared magnitude of the wave function ψ associated with the largest β_n

Figure 6.2: Finite aperiodic square moiré lattice, with $\tan(\theta) = \sqrt{3}$. Different values of p_2 are compared: 0.1 (left) and 0.4 (right).

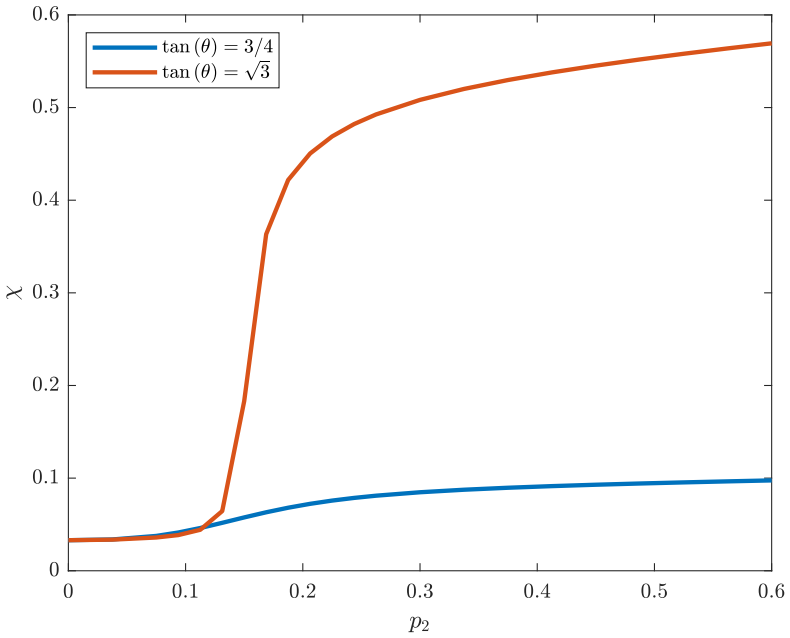

Figure 6.3: χ as a function of p_2 for selected periodic (blue) and aperiodic (orange) square moiré lattices.

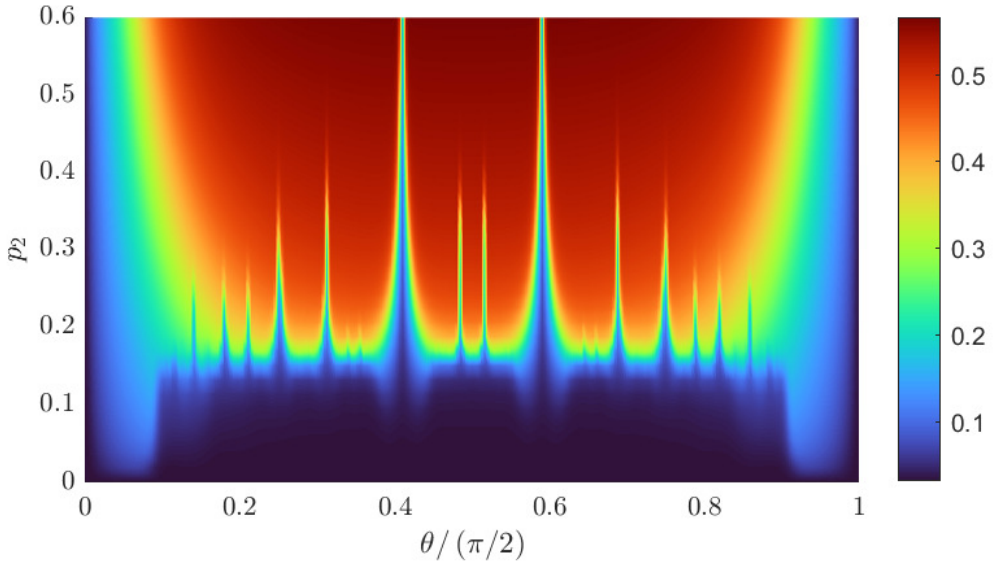

Figure 6.4: χ as a function of θ and p_2 for square moiré lattices.

6.2 Hexagonal

Hexagonal moiré lattices are similar to square ones, given that the only parameter is the length of the primitive lattice vectors, which in this case is fixed by the primitive cell area. Localization and delocalization occur for approximately the same values of p_2 as the square case. Figure 6.5 shows a comparison of a periodic and an aperiodic potential, both with $p_2 = 0.4$. For the periodic case, $\tan(\theta) = 4\sqrt{3}$, while for the aperiodic one, $\tan(\theta) = 1$. The corresponding measures of localization are $\chi \approx 0.1$ and $\chi \approx 0.5$, respectively.

An overview of the localization-delocalization transition for these two examples can be analyzed in Figure 6.6. While the periodic potential is poorly localized for all p_2 in the considered interval, the aperiodic potential becomes localized at $p_2^{\mathrm{LDT}} \approx 0.16$. This behavior is similar to the one found in the square lattice. Finally, a global picture of χ as a function of θ and p_2 is presented in Figure 6.7, where it is possible to observe that p_2^{LDT} does not depend very strongly on θ.

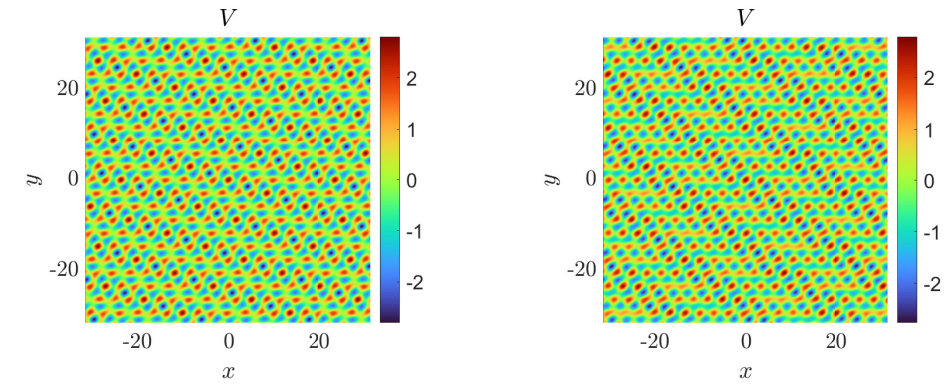

(a) Potential $V(x,y)$

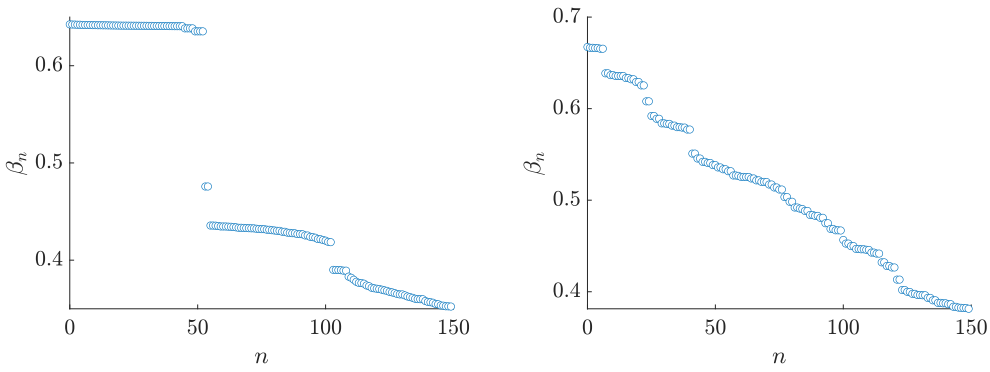

(b) Propagation constants β_n, in descending order

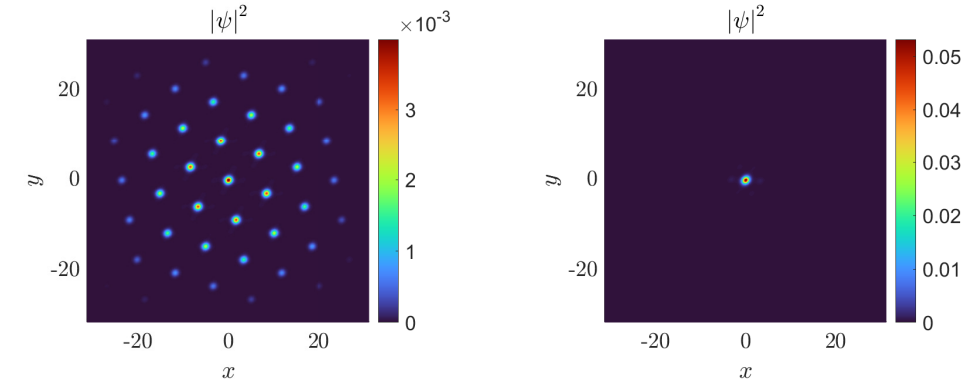

(c) Squared magnitude of the wave function ψ associated with the largest β_n

Figure 6.5: Finite hexagonal moiré lattice, with $p_2 = 0.4$. For the periodic lattice (left), $\tan(\theta) = 4\sqrt{3}$. For the aperiodic lattice (right), $\tan(\theta) = 1$.

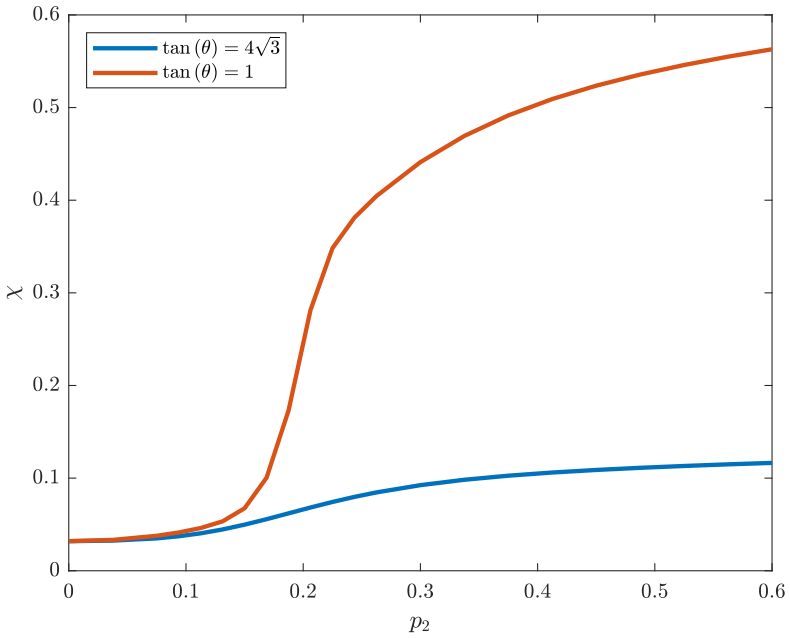

Figure 6.6: χ as a function of p_2 for selected periodic (blue) and aperiodic (orange) hexagonal moiré lattices.

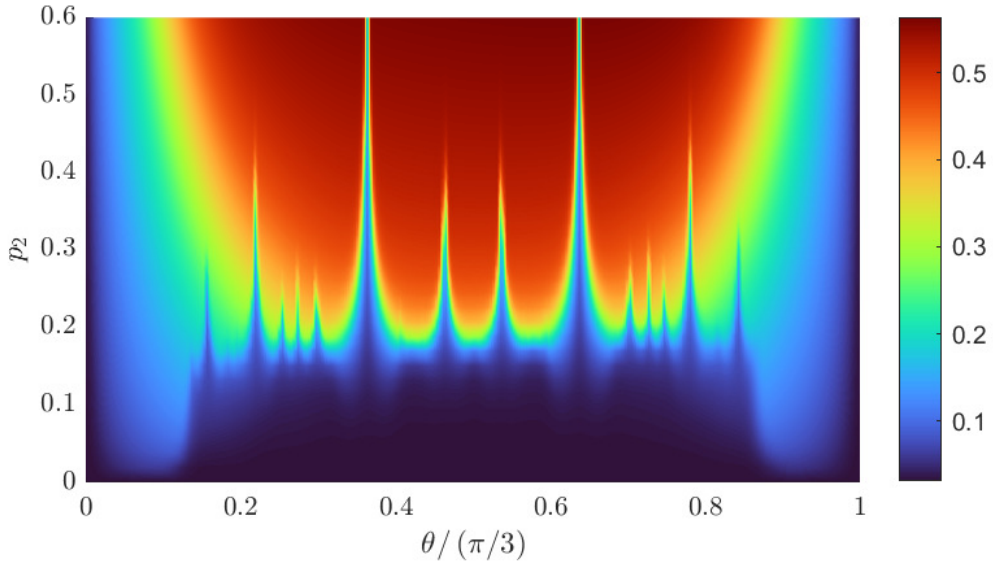

Figure 6.7: χ as a function of θ and p_2 for hexagonal moiré lattices.

6.3 Rectangular

Rectangular moiré lattices introduce an additional parameter, α, the ratio of lengths of the primitive lattice vectors. Based on the condition derived on Section 5.3.1, two values of α were chosen for the examples: $\sqrt{2}$ and π.

For $\alpha = \sqrt{2}$, it is possible to obtain a periodic or an aperiodic lattice. Figure 6.8 presents results for periodic and aperiodic potentials, which are comparable to the square and hexagonal examples. In both cases, $p_2 = 0.4$. For the periodic potential, $\tan(\theta) = 2\sqrt{2}$, while for the aperiodic one, $\tan(\theta) = 1$. The corresponding measures of localization are $\chi \approx 0.06$ and $\chi \approx 0.52$, respectively.

For $\alpha = \pi$, however, there is a special case with one-dimensional periodicity, shown in Figure 6.9, which requires a higher value of p_2. In the example, $p_2 = 0.8$ and $\tan(\theta) = 4\pi/\left(4-\pi^2\right)$. The measure of localization is $\chi \approx 0.18$. It is still possible to localize the wave with an aperiodic potential, as presented in Figure 6.9, where $p_2 = 0.4$, $\tan(\theta) = 1$, and $\chi \approx 0.36$.

An overview of the localization-delocalization transition for these four examples can be analyzed in Figure 6.10. As expected, the periodic potential is poorly localized for all p_2 in the considered interval. The one-dimensional periodic potential has corresponding values of χ which are higher than the periodic case, but lower than the aperiodic ones, due to localization in one dimension and delocalization in the other. The aperiodic potential for $\alpha = \sqrt{2}$ behaves similarly to square and hexagonal aperiodic potentials. The aperiodic potential for $\alpha = \pi$ is also localized, but χ is lower.

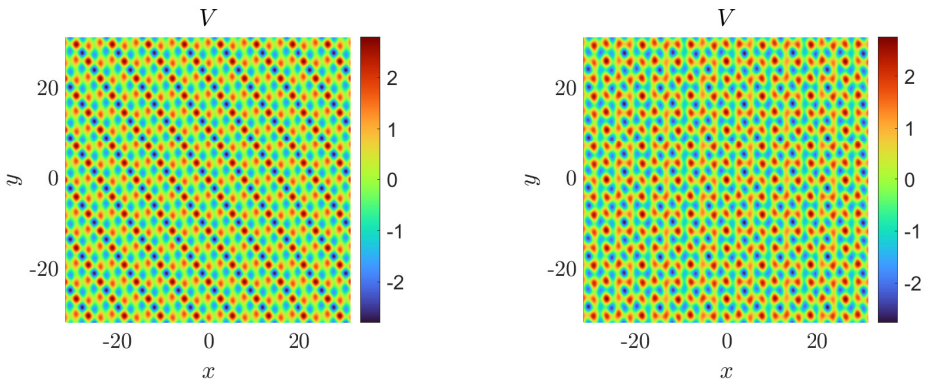

(a) Potential $V(x,y)$

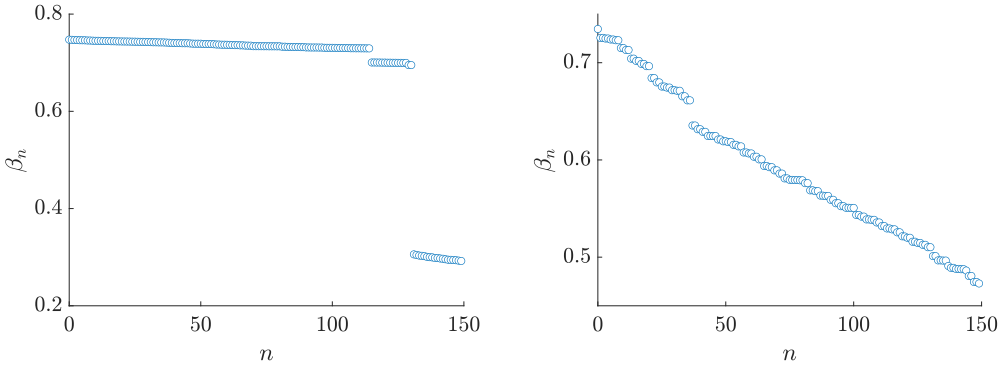

(b) Propagation constants β_n, in descending order

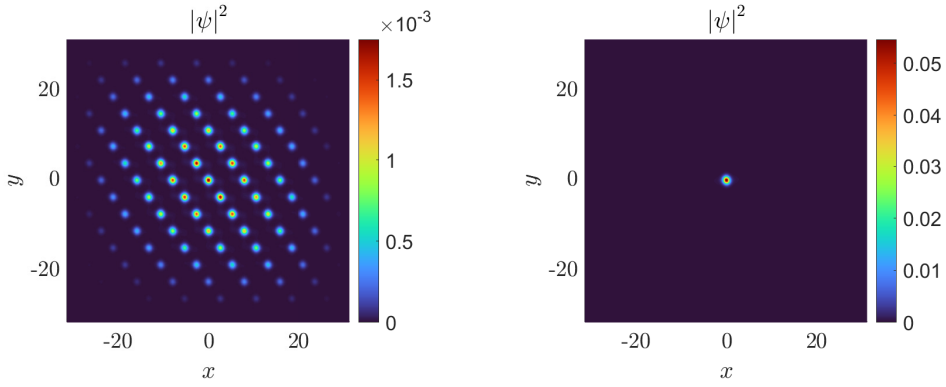

(c) Squared magnitude of the wave function ψ associated with the largest β_n

Figure 6.8: Finite rectangular moiré lattice, with $\alpha^2 = 2$ and $p_2 = 0.4$. For the periodic lattice (left), $\tan(\theta) = 2\sqrt{2}$. For the aperiodic lattice (right), $\tan(\theta) = 1$.

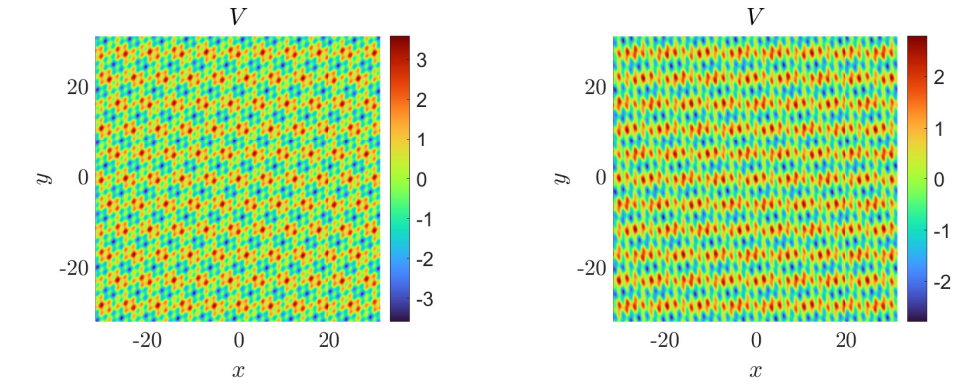

(a) Potential $V(x,y)$

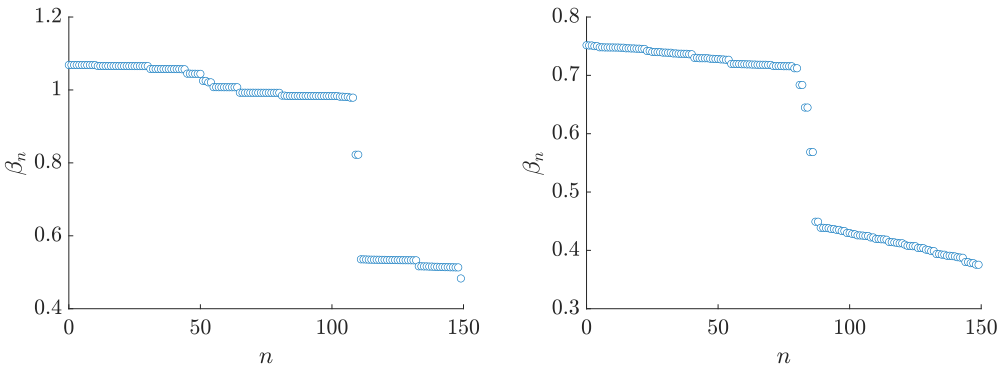

(b) Propagation constants β_n, in descending order

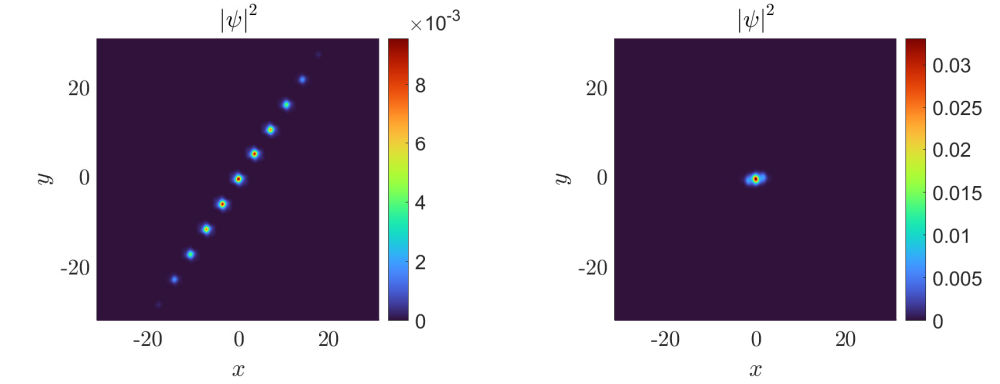

(c) Squared magnitude of the wave function ψ associated with the largest β_n

Figure 6.9: Finite rectangular moiré lattice, with $\alpha^2 = \pi^2$. For the one-dimensional periodic lattice (left), $\tan(\theta) = 4\pi/\left(4-\pi^2\right)$ and $p_2 = 0.8$. For the aperiodic lattice (right), $\tan(\theta) = 1$ and $p_2 = 0.4$.

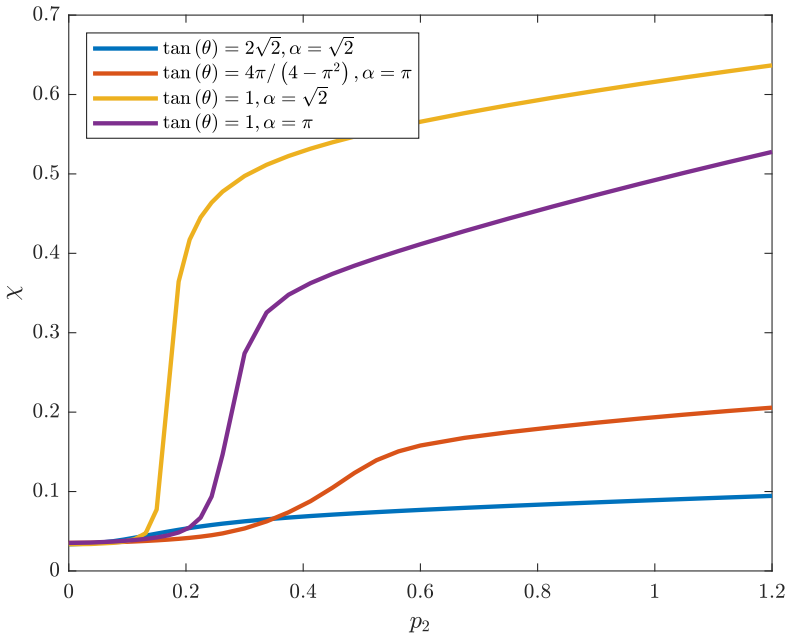

Figure 6.10: χ as a function of p_2 for selected periodic (blue), one-dimensional periodic (orange), and aperiodic (yellow and purple) rectangular moiré lattices.

6.4 Centered Rectangular

Like rectangular moiré lattices, centered rectangular have an additional parameter, in this case, φ, the angle between the primitive lattice vectors. Based on the condition derived on Section 5.4.1, two values of φ were chosen for the examples: $\arccos(1/3)$ and $\pi/6$. For $\varphi = \arccos(1/3)$, it is possible to obtain a periodic or aperiodic lattice. Figure 6.11 presents results for periodic and aperiodic potentials, which are comparable to the square and hexagonal examples. In both cases, $p_2 = 0.4$. For the periodic potential, $\tan(\theta) = 2\sqrt{2}$, while for the aperiodic one, $\tan(\theta) = 1$.

For $\varphi = \pi/6$, however, there is a special case with one-dimensional periodicity, shown in Figure 6.12, which requires a higher value of p_2. In the example, $p_2 = 1.6$ and $\tan(\theta) = -3/11\left(5\sqrt{3}+8\right)$, corresponding to $\chi \approx 0.24$. It is still possible to localize the wave with an aperiodic potential, as presented in Figure 6.12, where $p_2 = 1.6$, $\tan(\theta) = 1$, and $\chi \approx 0.7$. However, unlike the rectangular moiré lattice, there is an interval of values of p_2 which results in wave localization in one dimension only, despite the aperiodic potential. Figure 6.13 illustrates this effect, comparing the localized case with a one-dimensional localized case obtained for similar parameters except for $p_2 = 0.8$, resulting in $\chi \approx 0.28$.

An overview of the localization-delocalization transition for these four examples can be analyzed in Figure 6.14. As expected, the periodic potential is poorly localized for all p_2 in the considered interval. The one-dimensional periodic potential has corresponding values of χ which are higher than the periodic case, but lower than the aperiodic ones, due to localization in one dimension and delocalization in the other. The aperiodic potential for $\varphi = \pi/6$ behaves very differently when compared to square, hexagonal, and rectangular moiré lattices. There is a value of p_2 above which the wave localizes only in one dimension, and a higher value of p_2 above which the wave localizes in both dimensions. In fact, for the aperiodic cases, χ is higher for $\varphi = \pi/6$ than for $\varphi = \arccos(1/3)$, for p_2 above approximately 1.2. Both cases with $\varphi = \pi/6$ appear to have a larger slope $\frac{\partial \chi}{\partial p_2}$ between $p_2 \approx 0.4$ and $p_2 \approx 1.4$.

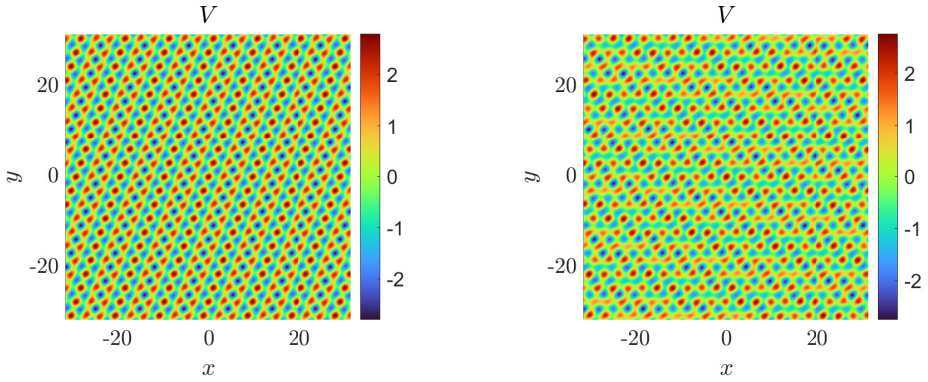

(a) Potential $V(x,y)$

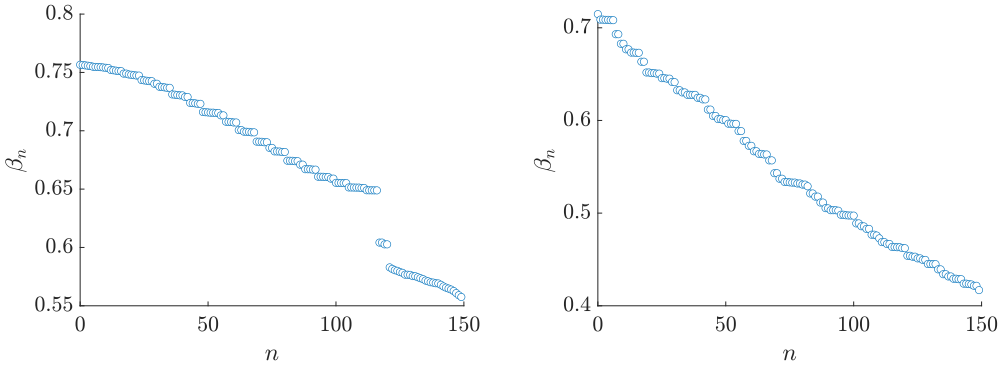

(b) Propagation constants β_n, in descending order

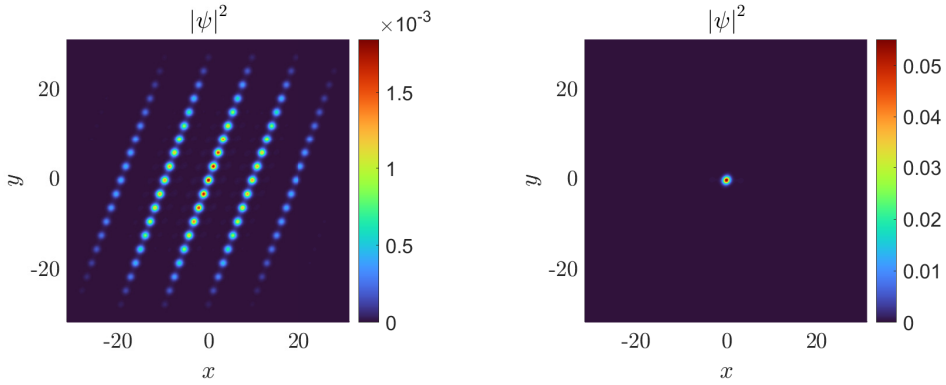

(c) Squared magnitude of the wave function ψ associated with the largest β_n

Figure 6.11: Finite rectangular moiré lattice, with $\cos(\varphi) = 1/3$ and $p_2 = 0.4$. For the periodic lattice (left), $\tan(\theta) = 2\sqrt{2}$. For the aperiodic lattice (right), $\tan(\theta) = 1$.

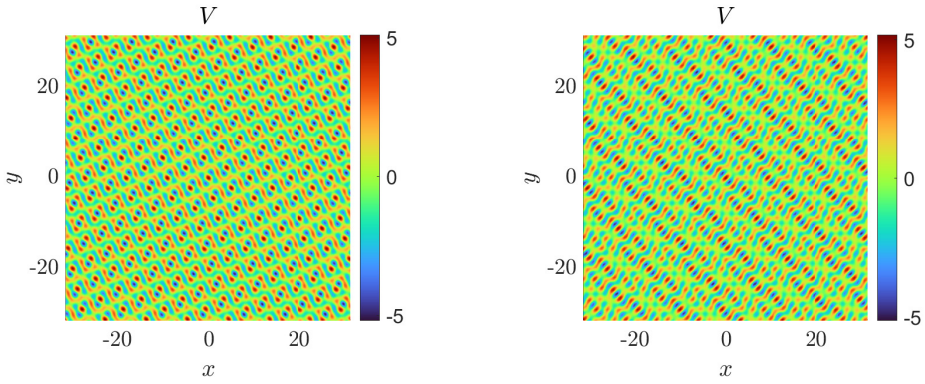

(a) Potential $V(x,y)$

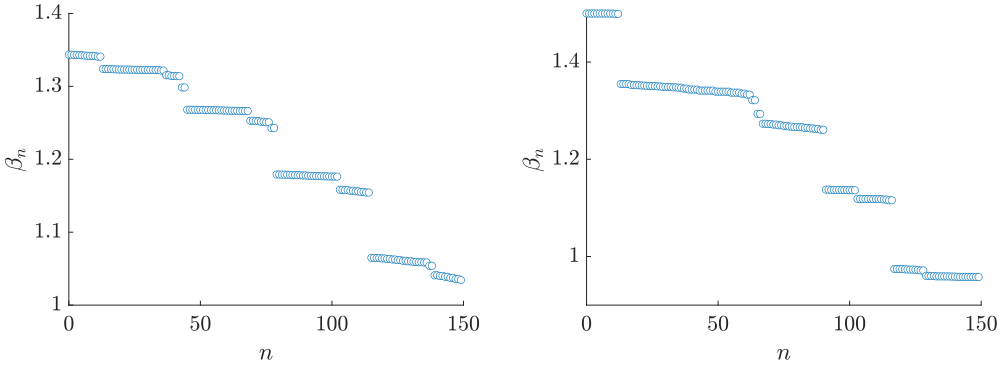

(b) Propagation constants β_n, in descending order

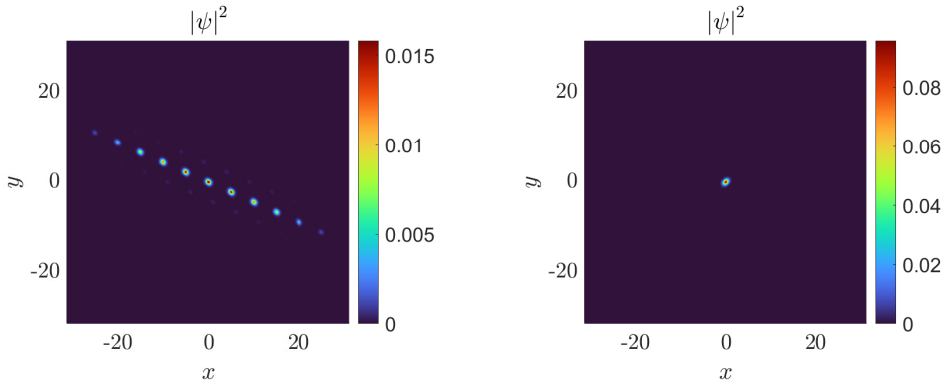

(c) Squared magnitude of the wave function ψ associated with the largest β_n

Figure 6.12: Finite rectangular moiré lattice, with $\cos(\varphi) = \sqrt{3}/2$ and $p_2 = 1.6$. For the one-dimensional periodic lattice (left), $\tan(\theta) = -3/11\left(5\sqrt{3}+8\right)$, $p_2 = 1.6$. For the aperiodic lattice (right), $\tan(\theta) = 1$.

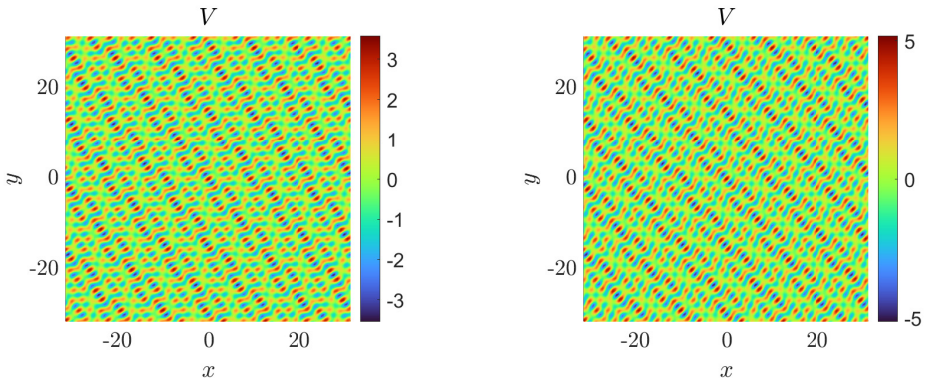

(a) Potential $V(x,y)$

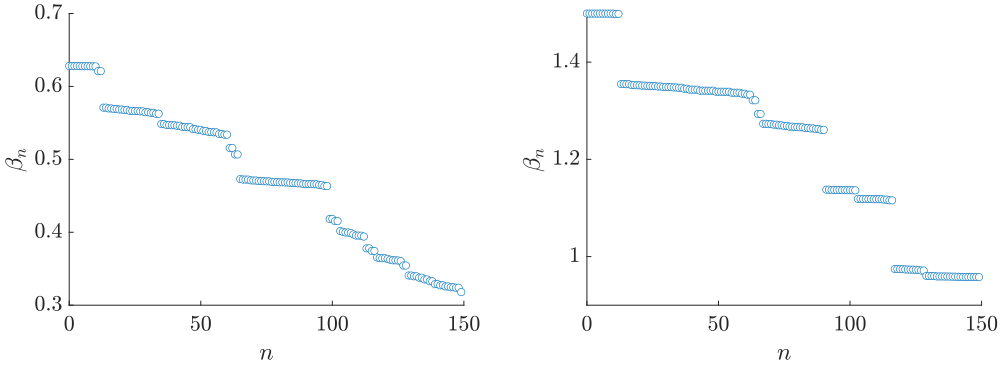

(b) Propagation constants β_n, in descending order

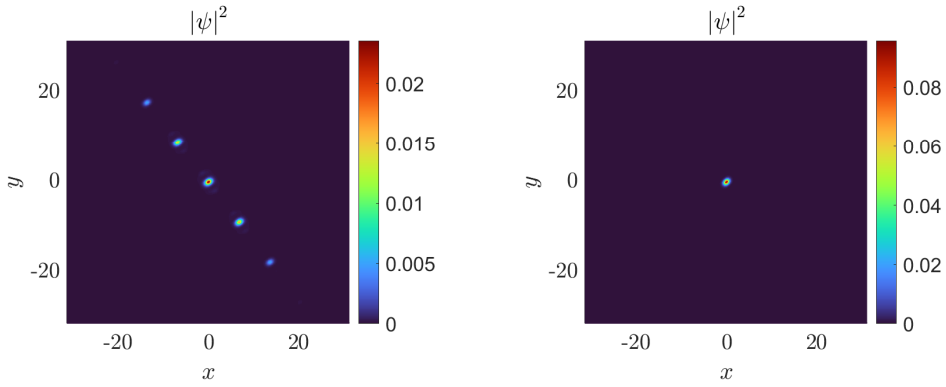

(c) Squared magnitude of the wave function ψ associated with the largest β_n

Figure 6.13: Finite aperiodic rectangular moiré lattice, with $\cos(\varphi) = \sqrt{3}/2$ and $\tan(\theta) = 1$. Different values of p_2 are compared: 0.8 (left) and 1.6 (right).

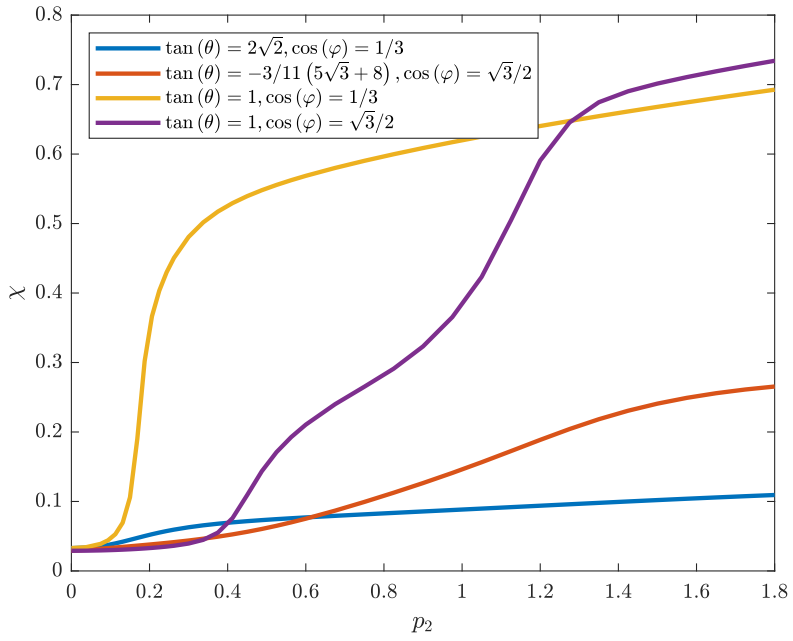

Figure 6.14: χ as a function of p_2 for selected periodic (blue), one-dimensional periodic (orange), and aperiodic (yellow and purple) rectangular moiré lattices.

6.5 Summary

This chapter considers wave propagation in potentials supported by moiré lattices in a finite area. Unlike the previous chapter, the lattice does not have to be periodic, so aperiodic and one-dimensional periodic potentials are explored as well. As expected, it is possible to verify that wave localization only occurs for aperiodic potentials with appropriate sublattice intensities. However, an interesting result is presented: it is possible to obtain a double transition, i.e. from unlocalized to one-dimensional localized and from one-dimensional localized to localized, which depends only on the intensity of the sublattices.

The next chapter introduces the possibility of wave localization in the edges and corners of moiré lattices, corresponding to propagation constants which are not the largest one.

Chapter 7

Truncated Moiré Lattices and Edge Localization

To investigate edge localization in truncated moiré lattices, the considered sublattice potential is the repetition over all lattice points of the Gaussian potential

$$G(x,y) = e^{-\left(\frac{x^2}{w_x^2}+\frac{y^2}{w_y^2}\right)} \tag{7.1}$$

where w_x and w_y define the width of the function in x and y, respectively. The lattice points can be represented by a kernel

$$K_m(x,y) = \sum_{n_v=-\infty}^{+\infty}\sum_{n_u=-\infty}^{+\infty} \delta\left(\begin{bmatrix}x\\y\end{bmatrix} - A_m\begin{bmatrix}n_u\\n_v\end{bmatrix}\right) \tag{7.2}$$

where A_m, for $m=1$ or $m=2$, is the basis matrix for each sublattice, described in Section 4.1. Finally, the repetition is the two-dimensional convolution in Cartesian coordinates x,y, represented as $**$, of the potential $G(x,y)$ with the truncated moiré combination of the sublattice kernels, which yields the potential

$$V(x,y) = G(x,y) ** \left[\text{rect}\left(\frac{x}{L_x}\right)\text{rect}\left(\frac{y}{L_y}\right)(p_1K_1(x,y)+p_2K_2(x,y))\right] \tag{7.3}$$

where L_x and L_y are the lengths that define the region of the lattice to keep in x and y. The length of the primitive lattice vectors is w_s and the basis matrices are the same as the ones considered in Chapter 6, except that the primitive cell area is now w_s^2. The examples in this chapter will consider $w_x = 0.25$, $w_y = 0.75$, $w_s = 3.3$, and $p_1 = p_2 = 1.95$, similar to [23].

In [23], edge localization is explored for a periodic lattice with periodic edges. This chapter presents results obtained for this case, as well as the other two possible cases: periodic lattice with aperiodic edges and aperiodic lattice with aperiodic edges. When the lattice is periodic, its orientation relative to the edges of the region that truncates it defines if the edge is periodic, i.e. if there is a lattice vector parallel to that edge. This orientation can be changed by globally rotating

the moiré lattice.

Similar to Chapter 6, the PDE is solved using the finite differences method, with zero boundary conditions.

7.1 Periodic Lattice with Periodic Edges

This case has been studied in [23] and its results are reproduced in Figures 7.1 and 7.2. In these cases, $\tan(\theta) = 3/4$, and the sublattice associated with basis matrix A_1 is aligned with the considered edges, i.e. there are lattice vectors that are parallel to the edges, in this case, they are the primitive vectors. This implies that the moiré lattice also has vectors that are parallel to the edges which, in this case, correspond to points on the considered edges and their intersections (corners). In (c) and (d), the orange points correspond to the selected wave profiles in (b). The mode with the largest β_n is delocalized, as expected, but there are localized modes at the edges of the lattice. Similar wave profiles appear in both cases, with strong localization.

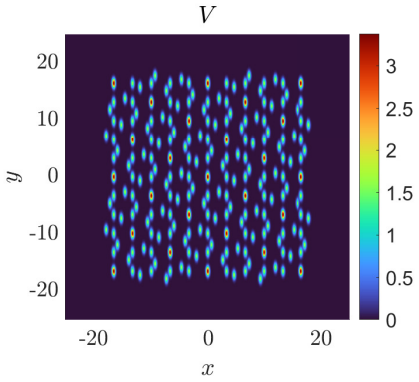

(a) Potential $V(x,y)$

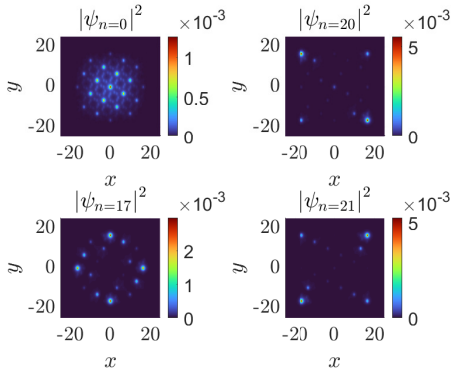

(b) Squared magnitude of selected wave functions ψ_n associated with propagation constants β_n

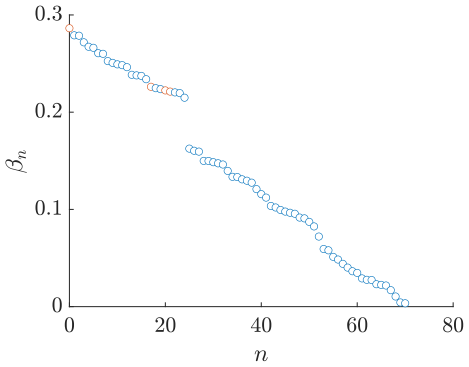

(c) Propagation constants β_n, in descending order

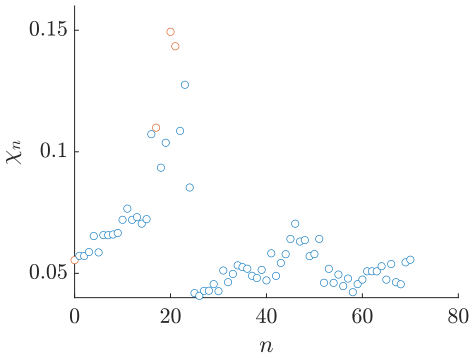

(d) Integral form factors χ_n associated with propagation constants β_n

Figure 7.1: Truncated periodic square moiré lattice with periodic edge, $\tan(\theta) = 3/4$, $L_x = L_y = 11w_s$.

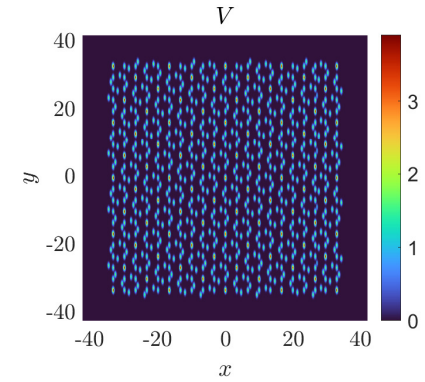

(a) Potential $V(x,y)$

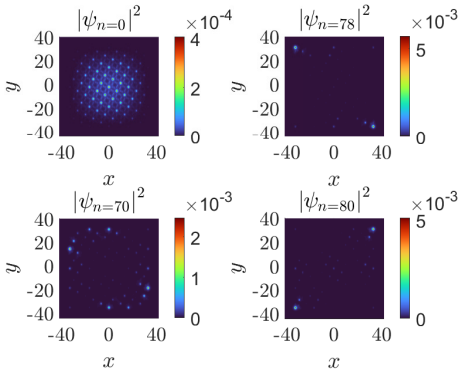

(b) Squared magnitude of selected wave functions ψ_n associated with propagation constants β_n

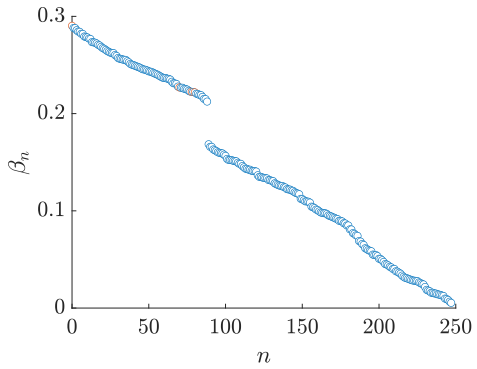

(c) Propagation constants β_n, in descending order

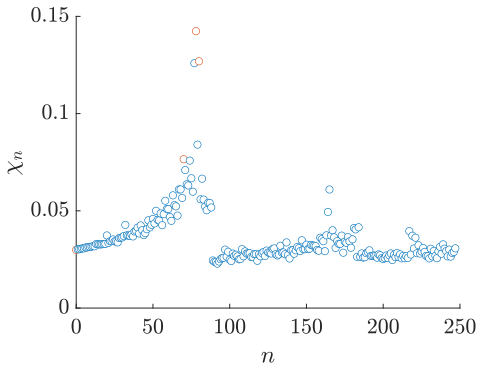

(d) Integral form factors χ_n associated with propagation constants β_n

Figure 7.2: Truncated periodic square moiré lattice with periodic edges, $\tan(\theta) = 3/4$, $L_x = L_y = 21w_s$.

7.2 Periodic Lattice with Aperiodic Edges

Figure 7.3 presents the obtained results for an aperiodic edge, obtained for $\tan(\theta) = 3/4$ and a global rotation by $\pi/4 - \pi/30$. Although some modes have a corresponding χ_n that is significantly larger than others, their wave profiles do not appear to be localized. The dimensions of the considered region are different when compared to the previous cases due to computational resource limitations.

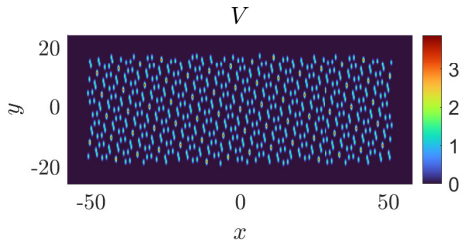

(a) Potential $V(x,y)$

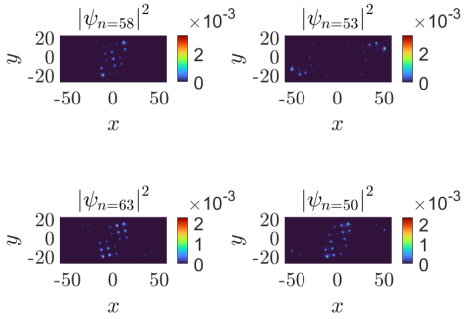

(b) Squared magnitude of selected wave functions ψ_n associated with propagation constants β_n

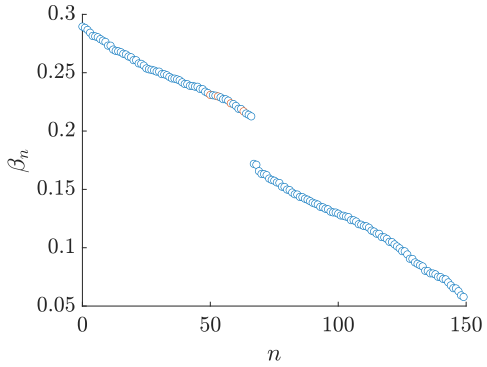

(c) Propagation constants β_n, in descending order

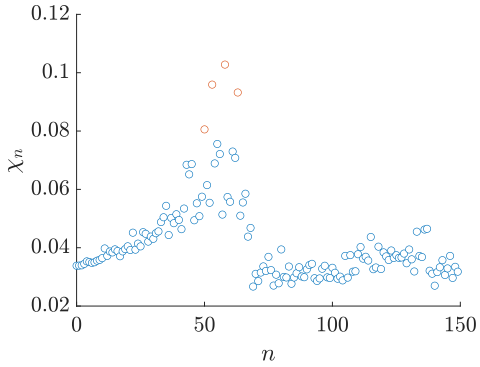

(d) Integral form factors χ_n associated with propagation constants β_n

Figure 7.3: Truncated periodic square moiré lattice with aperiodic edges, $\tan(\theta) = 3/4$, $L_x = 31w_s$, $L_y = 11w_s$, globally rotated by $\pi/4 - \pi/30$.

7.3 Aperiodic Lattice with Aperiodic Edges

When the lattice is aperiodic, all edges are aperiodic. An example is shown in Figure 7.4, where $\theta = \arctan(3/4) + \pi/30$ and the moiré lattice was globally rotated by $\pi/4$. In this case, the modes with the largest χ_n are not as significantly larger as in the previous case, but the wave profiles appear to be more localized.

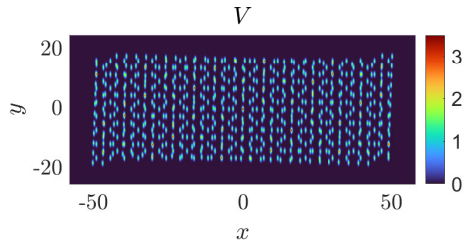

(a) Potential $V(x,y)$

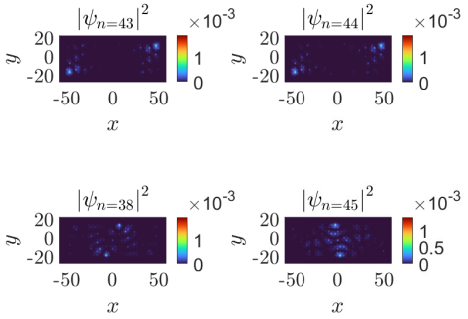

(b) Squared magnitude of selected wave functions ψ_n associated with propagation constants β_n

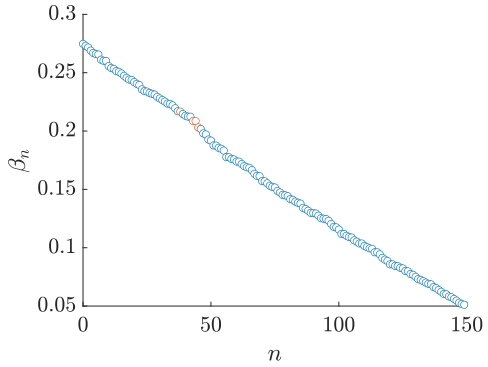

(c) Propagation constants β_n, in descending order

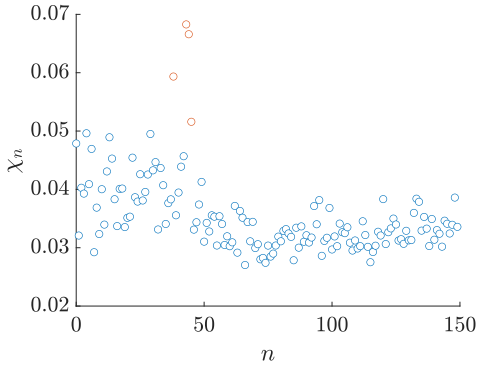

(d) Integral form factors χ_n associated with propagation constants β_n

Figure 7.4: Truncated aperiodic square moiré lattice with aperiodic edges, $\theta = \arctan(3/4) + \pi/30$, $L_x = 31w_s$, $L_y = 11w_s$, globally rotated by $\pi/4$.

7.4 Summary

This chapter explores the most localized wave propagation modes of potentials supported by moiré lattices, using the integral form factor χ as the measure of localization. For periodic moiré lattices with periodic edges, these modes are mostly localized in the edges of the lattice. However, for moiré lattices, either periodic or aperiodic, with aperiodic edges, the most localized modes have a value of χ that is not significantly higher than for other modes, and the wave profiles do not appear to be localized, except for aperiodic lattices.

Chapter 8

Conclusions and Future Work

A flexible algorithm was implemented, following a carefully designed methodology, whose most relevant aspects are described in Chapter 4. It allows computing propagation constants and wave profiles for different potentials, using the chosen numerical algorithm and boundary conditions. It also comprises a set of lattice analyses that can be performed, so that the obtained results are more consistent and easier to compute. Furthermore, unit tests were implemented, to validate the correctness of the algorithm.

The study of periodic moiré lattices and their properties was performed for square, hexagonal, rectangular, and centered rectangular moiré lattices. Square and hexagonal lattices only have two parameters: the length of the primitive vectors, and the relative rotation angle, θ. Rectangular and centered rectangular lattices have an additional parameter: the ratio of lengths of the primitive vectors, or the angle between them, respectively. This additional parameter introduces an additional condition for the periodicity of the moiré lattice. If this condition is verified, the periodicity of these lattices is similar to square and hexagonal ones: $\tan(\theta)$ can be obtained from parameters $a, b \in \mathbb{Z}$, obtained from a homogeneous second-order Diophantine equation, specifically defined for each lattice, which is relatively easy to solve. The primitive lattice vectors can then be generated from a system of linear Diophantine equations, which is not trivial to solve for generic coefficients. However, for rectangular and centered rectangular lattices, if the additional condition is not verified, the resulting lattice may be either one-dimensional periodic or aperiodic. Some examples are presented for these periodic moiré lattices, and their respective band structure and representative wave profile are analyzed.

For finite lattices, with zero boundary conditions, the results found in the literature were reproduced for square and hexagonal moiré lattices: a localization-delocalization transition occurs if these lattices are aperiodic, depending only on the variation of the sublattice intensities. Additionally, for rectangular and centered rectangular moiré lattices, one-dimensional localization is shown to be possible, for one-dimensional periodic lattices. For centered rectangular lattices in particular, a double transition is also possible, when the additional periodicity condition is not verified, and the potential is aperiodic: the variation of the sublattice intensity can transition from unlocalized to one-dimensional localized, and from one-dimensional localized to localized.

Finally, modes that are localized at the edges or corners of the lattice were studied. Localization in the periodic edges of periodic lattices is possible, as presented in the literature. However, no example of edge or corner localization was found for aperiodic edges on either periodic or aperiodic lattices.

8.1 Future Work

This work explored wave localization in square, hexagonal, rectangular, and centered rectangular moiré lattices, with rotation around the origin, according to the linear Schrödinger equation. As such, the following topics should be studied in the future:

- Oblique moiré lattices;
- Moiré lattices obtained from the rotation of Bravais lattices around arbitrary points;
- Non-linear wave equation including, for example, soliton formation.

Finally, an article is being prepared with the results presented in this document, as well as considering non-linear effects in the wave equation.

References

[1] Björn Lechthaler, Christoph Pauly, and Frank Mücklich. Objective homogeneity quantification of a periodic surface using the gini coefficient. *Scientific Reports*, 10:14516, 2020. doi:10.1038/s41598-020-70758-9.

[2] Charles Kittel. *Introduction to solid state physics*. John Wiley, Hoboken, N.J, 8th edition, 2005.

[3] C. M. Huang, F. W. Ye, X. F. Chen, Y. V. Kartashov, V. V. Konotop, and L. Torner. Localization-delocalization wavepacket transition in pythagorean aperiodic potentials. *Scientific Reports*, 6, 2016. doi:10.1038/srep32546.

[4] P. Wang, Y. Zheng, X. Chen, C. Huang, Y. V. Kartashov, L. Torner, V. V. Konotop, and F. Ye. Localization and delocalization of light in photonic moiré lattices. *Nature*, 577(7788):42–46, 2019. doi:10.1038/s41586-019-1851-6.

[5] C. R. Dean, L. Wang, P. Maher, C. Forsythe, F. Ghahari, Y. Gao, J. Katoch, M. Ishigami, P. Moon, M. Koshino, T. Taniguchi, K. Watanabe, K. L. Shepard, J. Hone, and P. Kim. Hofstadter's butterfly and the fractal quantum hall effect in moire superlattices. *Nature*, 497(7451):598–602, 2013. doi:10.1038/nature12186.

[6] R. Bistritzer and A. H. MacDonald. Moire bands in twisted double-layer graphene. *Proceedings of the National Academy of Sciences of the United States of America*, 108(30):12233–12237, 2011. doi:10.1073/pnas.1108174108.

[7] Y. Cao, V. Fatemi, S. Fang, K. Watanabe, T. Taniguchi, E. Kaxiras, and P. Jarillo-Herrero. Unconventional superconductivity in magic-angle graphene superlattices. *Nature*, 556(7699):43–+, 2018. doi:10.1038/nature26160.

[8] Y. Cao, V. Fatemi, S. Fang, K. Watanabe, T. Taniguchi, E. Kaxiras, and P. Jarillo-Herrero. Unconventional superconductivity in magic-angle graphene superlattices. *Nature*, 556(7699):43–50, 2018. doi:10.1038/nature26160.

[9] Q. Fu, P. Wang, C. Huang, Y. V. Kartashov, L. Torner, V. V. Konotop, and F. Ye. Optical soliton formation controlled by angle twisting in photonic moiré lattices. *Nature Photonics*, 14(11):663–668, 2020. doi:10.1038/s41566-020-0679-9.

[10] Y. V. Kartashov, F. Ye, V. V. Konotop, and L. Torner. Multifrequency solitons in commensurate-incommensurate photonic moiré lattices. *Physical Review Letters*, 127(16), 2021. doi:10.1103/PhysRevLett.127.163902.

[11] F. Bloch. About the quantum mechanics of electrons in crystal lattices. *Zeitschrift Fur Physik*, 52(7-8):555–600, 1929. doi:10.1007/bf01339455.

[12] P. W. Anderson. Absence of diffusion in certain random lattices. *Physical Review*, 109(5):1492–1505, 1958. doi:10.1103/PhysRev.109.1492.

[13] J. Bareño-Silva, F. J. Caro-Lopera, H. A. Gómez-Urrea, and M. E. Mora-Ramos. Narrow band filter designed from bravais-moiré two-dimensional photonic crystal. *Photonics and Nanostructures - Fundamentals and Applications*, 52, 2022. doi:10.1016/j.photonics.2022.101082.

[14] Y. V. Kartashov. Light bullets in moiré lattices. *Optics Letters*, 47(17):4528–4531, 2022. doi:10.1364/OL.471022.

[15] T. H. Talukdar, A. L. Hardison, and J. D. Ryckman. Moiré effects in silicon photonic nanowires. *ACS Photonics*, 9(4):1286–1294, 2022. doi:10.1021/acsphotonics.1c01800.

[16] N. S. Salakhova, I. M. Fradkin, S. A. Dyakov, and N. A. Gippius. Twist-tunable moire optical resonances. *Physical Review B*, 107(15), 2023. doi:10.1103/PhysRevB.107.155402.

[17] T. Ning, Y. Ren, Y. Huo, and Y. Cai. Efficient high harmonic generation in nonlinear photonic moiré superlattice. *Frontiers of Physics*, 18(5), 2023. doi:10.1007/s11467-023-1296-0.

[18] J. Zhou, S. Xie, C. Nie, P. Xu, J. Yi, and E. Liu. Optical properties of a moiré-lattice photonic crystal fiber with controllable magic angle. *Results in Physics*, 51, 2023. doi:10.1016/j.rinp.2023.106659.

[19] H. Tang, X. Ni, F. Du, V. Srikrishna, and E. Mazur. On-chip light trapping in bilayer moiré photonic crystal slabs. *Applied Physics Letters*, 121(23), 2022. doi:10.1063/5.0105365.

[20] H. A. Gómez-Urrea, M. C. Ospina-Medina, J. D. Correa-Abad, M. E. Mora-Ramos, and F. J. Caro-Lopera. Tunable band structure in 2d bravais–moiré photonic crystal lattices. *Optics Communications*, 459, 2020. doi:10.1016/j.optcom.2019.125081.

[21] R. Decker, Y. Wang, V. W. Brar, W. Regan, H. Z. Tsai, Q. Wu, W. Gannett, A. Zettl, and M. F. Crommie. Local electronic properties of graphene on a bn substrate via scanning tunneling microscopy. *Nano Letters*, 11(6):2291–2295, 2011. doi:10.1021/nl2005115.

[22] C. R. Woods, L. Britnell, A. Eckmann, R. S. Ma, J. C. Lu, H. M. Guo, X. Lin, G. L. Yu, Y. Cao, R. V. Gorbachev, A. V. Kretinin, J. Park, L. A. Ponomarenko, M. I. Katsnelson, Yu N. Gornostyrev, K. Watanabe, T. Taniguchi, C. Casiraghi, H. J. Gao, A. K. Geim, and K. S. Novoselov. Commensurate-incommensurate transition in graphene on hexagonal boron nitride. *Nature Physics*, 10(6):451–456, 2014. doi:10.1038/nphys2954.

[23] A. A. Arkhipova, Y. V. Kartashov, S. K. Ivanov, S. A. Zhuravitskii, N. N. Skryabin, I. V. Dyakonov, A. A. Kalinkin, S. P. Kulik, V. O. Kompanets, S. V. Chekalin, F. Ye, V. V. Konotop, L. Torner, and V. N. Zadkov. Observation of linear and nonlinear light localization at the edges of moiré arrays. *Physical Review Letters*, 130(8), 2023. doi:10.1103/PhysRevLett.130.083801.

[24] Calvin T Long. *Elementary Introduction to Number Theory (2nd ed.)*. Lexington: D. C. Heath and Company, 1972.